3-22-2012

A Quantitative Analysis of Solar Flare Characteristics as Observed in the Solar Observing Optical Network and the Global Oscillation Network Group

Thomas M. Wittman

A QUANTITATIVE ANALYSIS OF SOLAR FLARE CHARACTERISTICS AS OBSERVED IN THE SOLAR OBSERVING OPTICAL NETWORK AND THE GLOBAL OSCILLATION NETWORK GROUP

THESIS

Thomas M. Wittman, Captain, USAF

AFIT/APPLPHY/ENP/12-M11

DEPARTMENT OF THE AIR FORCE
AIR UNIVERSITY

AIR FORCE INSTITUTE OF TECHNOLOGY

Wright-Patterson Air Force Base, Ohio

AFIT/APPLPHY/ENP/12-M11

A QUANTITATIVE ANALYSIS OF SOLAR FLARE CHARACTERISTICS AS OBSERVED IN THE SOLAR OBSERVING OPTICAL NETWORK AND THE GLOBAL OSCILLATION NETWORK GROUP

THESIS

Presented to the Faculty

Department of Engineering and Physics

Graduate School of Engineering and Management

Air Force Institute of Technology

Air University

Air Education and Training Command

In Partial Fulfillment of the Requirements for the

Degree of Master of Science in Engineering Physics

Thomas M. Wittman, BS

Captain, USAF

March 2012

AFIT/APPLPHY/ENP/12-M11

A QUANTITATIVE ANALYSIS OF SOLAR FLARE CHARACTERISTICS AS OBSERVED IN THE SOLAR OBSERVING OPTICAL NETWORK AND THE GLOBAL OSCILLATION NETWORK GROUP

Thomas M. Wittman, BS

Captain, USAF

Approved:

Lt Col Ariel O. Acebal (Chairman)	9 MARCH 2012 Date
William F. Bailey, PhD (Member)	8 Mar 12 Date
Capt Matthew B. Garvin (Member)	9 Mar 12 Date
Carl J. Henney, PhD (Member)	2/28/2012 Date

Abstract

This study consists of a quantitative comparison of H-alpha solar flare area and brightness as recorded by the Solar Observing Optical Network (SOON) and the Global Oscillation Network Group (GONG) from March 11 through November 30, 2011. The Air Force utilizes the three-site SOON network for H-alpha flare monitoring, while the six-site GONG network, managed by the National Solar Observatory, provides backup H-alpha flare monitoring for SOON. A total of 1000 flares were observed and 100 of these were rated larger or brighter than the 0-F category. In the SOON network, 8% of flares observed by two sites had a difference in area or brightness category, or both. In the GONG network, with up to four sites viewing the same flare, 44% of flares observed by multiple sites had at least one site with differences in area, brightness, or both. Of these cases, the GONG site that rated the flare as having the largest or brightest rating also had the highest sharpness 95% of the time. Of the 84 flares larger or brighter than 0-F observed by both networks, area and brightness category ratings were the same 35% of the time. The GONG rating was one category larger or brighter than SOON 26% of the time and the SOON rating was one category larger or brighter than GONG 39% of the time. There was only one case with a two category difference between networks this was attributed to clouds at one site. GONG observed all 9 of SOON's event-level flares while observing three additional that SOON did not observe. Ultimately, GONG observed all SOON flares with the same variability noted when comparing flares observed within the SOON network, and is a reliable source for H-alpha flare observations.

Acknowledgments

I would like to express my honest appreciation to my faculty advisor, Lt Col Ariel Acebal, for his guidance throughout this thesis project. There were several opportunities where I could have gone astray yet he shepherded my efforts in the right direction. I must also extend a sincere thanks to my committee member Dr. Carl Henney at the Air Force Research Laboratory who was an immense help during my visit. Without his depth of knowledge and programming expertise this project would not have been possible. I also appreciate my other two committee members, Dr. William Bailey whose unique perspective helped me work through research problems, and Capt Matthew Garvin, who although joined my committee late in the process, provided appreciated encouragement and perspective.

I am also grateful to the warm welcome from all the folks at the AFWA Detachment 4 Solar Observatory at Holloman AFB. Especially for MSgt Shane Siebert for his hospitality and efforts to answer all of my questions and for John Pietrzak who although I never met in person really went out of his way to offer his assistance in whatever ways he could. I also appreciate the time and effort that the solar observatories at San Vito and Learmonth took to send me their solar imagery for many months on end.

Last but certainly not least, I need to thank my wonderful wife who despite the fact that she was also a full time student, did a phenomenal job of supporting me and making my life at home a relief from the stresses that come with being a graduate student. I am blessed to be her husband!

Thomas M. Wittman

Table of Contents

Page

List of Figures

Figure Page

List of Tables

A QUANTITATIVE ANALYSIS OF SOLAR FLARE CHARACTERISTICS AS OBSERVED IN THE SOLAR OBSERVING OPTICAL NETWORK AND THE GLOBAL OSCILLATION NETWORK GROUP

1. Introduction

1.1 Background

A solar flare is an intense brightening that occurs in the solar atmosphere when stored magnetic energy is released in an explosive manner. Most solar flares are accompanied by enhancements in the solar spectrum across a range of wavelengths from radio waves to X-rays and Gamma rays. The Hydrogen-alpha (H-alpha) emission line, 6562.8 Å, has long been used to grade the intensity of solar flares and continues to be utilized to this day. Flares are an important gauge of solar activity and alert forecasters to the possibility of impacts to the Earth's local space weather environment, including harmful effects on military and civilian operations.

The Air Force operates three optical solar observatories that comprise the Solar Observing Optical Network (SOON) which perform solar monitoring as part of the larger Solar Electro-Optical Network (SEON). The SOON sites currently provide continual solar flare monitoring in the H-alpha wavelength, however they are slated for upgrade with a new optical telescope. As the upgrade takes place there is still need for continual visible flare monitoring. This is being provided by the civilian Global Oscillation Network Group system of six global observatories operated by the National Solar

Observatory. The GONG sites have recently added the capability to observe the sun in H-alpha.

1.2 Research Objective

Since the H-alpha monitoring portion of the GONG mission is less than two years old, little is known about its operational flare observing capability as compared to the established SOON network. Does GONG observe as many flares as SOON observes? Are flares observed in GONG of similar area and brightness as flares observed by SOON? Where does GONG have better capability than SOON and where is SOON superior? Can a non-military system be relied upon to provide an important space weather product to the field? The objective of this research is to answer these questions through a comparison of SOON and GONG observations. In order to achieve this objective, solar flare area and brightness information is collected from SOON observatories during a nine month period and corresponding H-alpha imagery from GONG is analyzed for comparison. If it can be shown that GONG observes as many or more solar flares as SOON with similar area and brightness ratings then increased confidence in GONG will result.

1.3 Preview

The following chapters are an account of the research process that led to a comparison of the SOON and GONG systems, and a determination of the ability of GONG as an effective flare monitoring tool. The next chapter provides background information on solar flares, as well as a discussion of the characteristics of the two observing systems. Chapter 3 outlines the methodology behind the research, including

data collection and analysis procedures. Then Chapter 4 addresses the results found after comparing flare characteristics in the two observing networks. Finally, conclusions are drawn in Chapter 5, as well as recommendations for further study.

2. Literature Review

2.1 Chapter Overview

The purpose of this chapter is to provide the reader with background information necessary to understand this project. The first section describes the phenomenon of solar flares. The second and third sections describe the SOON and GONG instruments.

2.2 The Solar Flare Phenomenon

It was not until 1859 that the first independent observations of a solar flare were observed by the English astronomers R.C. Carrington and R. Hodgson (Carrington, 1859). Not only was this sighting significant because it was the first observation of a solar flare, but also because it was one of the most energetic flares ever recorded. This so called white-light flare was seen as a brightening across the continuum of visible wavelengths, and it is now known that only the most powerful flares are able to be observed in this manner. Since that time ever-increasing numbers of flares have been detected by scientists. With the advent of spaced-based observations in the 1960s, solar flares have also been observed to radiate in the extreme ultraviolet and X-ray realms, providing additional clues to the underlying physics behind these solar explosions.

A solar flare is a localized sudden brightening of the solar disk that is observable across virtually all wavelengths. Solar flares tend to be located near regions in the solar atmosphere where magnetic fields are strongest and most complex, called active regions. In the visible spectrum these active regions can be observed in conjunction with sunspots (Figure 1), where magnetic fields tend to suppress the underlying convection.

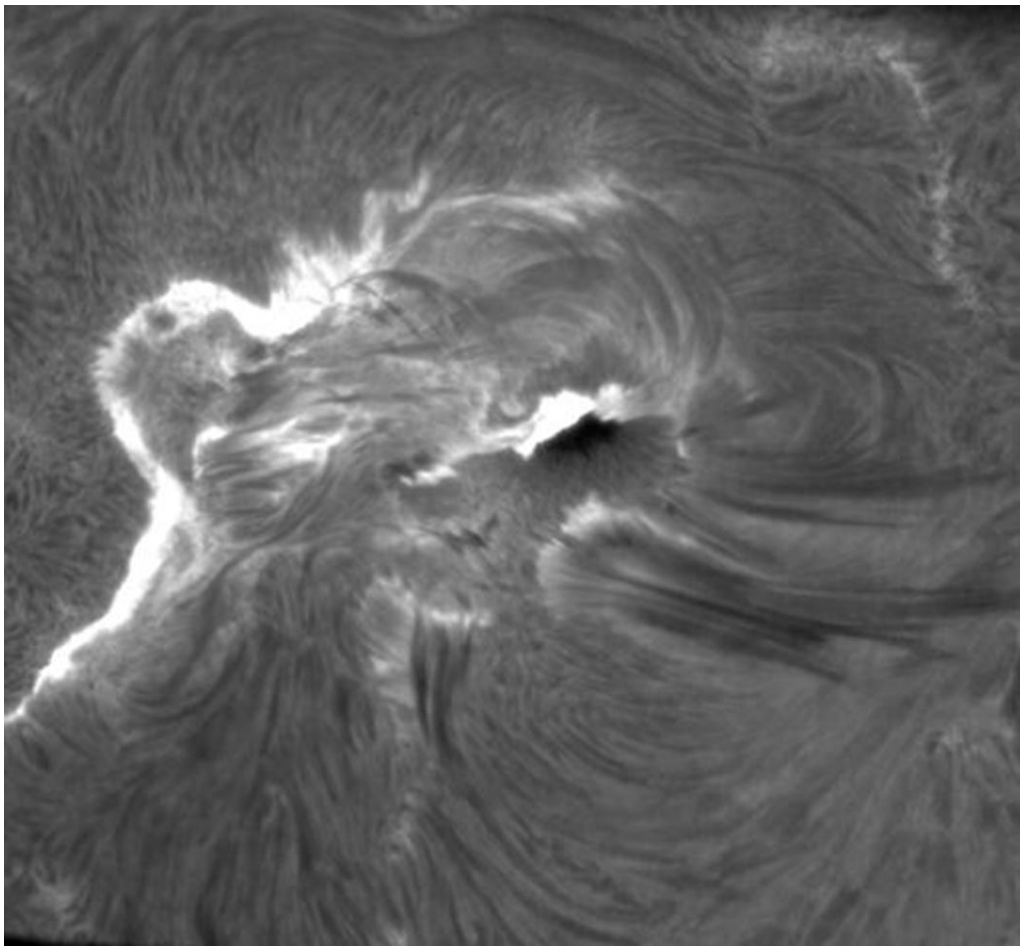

Figure 1. H-alpha Image of a Solar Flare. From Big Bear Solar Observatory, 5 November 1998. Note the sunspot associated with the locally enhanced magnetic field near the center of the image. Big Bear Solar Observatory (http://www.bbso.njit.edu/)

During a solar flare, the plasma is heated to tens of millions of degrees and elementary particles are accelerated to relativistic velocities (Lang, 2009). Although solar flares contain an increase in radiation across the electromagnetic spectrum, they are typically best seen in certain wavelengths where the relative brightening is greater, including H-alpha. There are also spectral line enhancements in the EUV and soft X-ray wavelengths, caused by the quantum transitions of highly ionized trace elements, such as

iron, which has dozens of emission lines (Harrison et al., 1997). A continuum of X-ray and Gamma-ray radiation is caused by various collisional processes as high energy particles accelerate down magnetic field lines into the lower chromosphere (Benz, 2008). On the other end of the spectrum, radio waves are produced by high speed electrons that are accelerated as they spiral around local magnetic field lines. Studying the electromagnetic radiation released by solar flares provides evidence of the underlying physics behind these energetic solar eruptions.

2.2.1 H-alpha Flare Characterization

Light in the H-alpha wavelength is emitted when a hydrogen atom transitions from a level of $n = 3$ to $n = 2$, and is part of the Balmer Series. In H-alpha, the flare appears as a sudden brightening on the chromospheric solar disk that gradually decays over times ranging from few minutes to a few hours in the case of intense flares. The magnetic footpoints of newly connected field lines are represented in H-alpha flares by brightenings in at least two distinct regions. These footpoints separate regions of opposite magnetic polarity, and often are extended along horizontal lines where H-alpha brightening occurs, termed flare ribbons (Foukal, 2004).

These H-alpha flare ribbons (Figure 2) are manifestations of the distribution of a flare's energy. After a flare takes place in the corona, particles are accelerated to relativistic velocities away from the initiation site, travelling down magnetic field lines into the chromosphere (Figure 3). This is where the flare ribbons are manifested, as ambient hydrogen decays after it has been ionized or excited. Flare ribbons are also seen in X-ray wavelengths where they map out the chromospheric footpoints of the newly

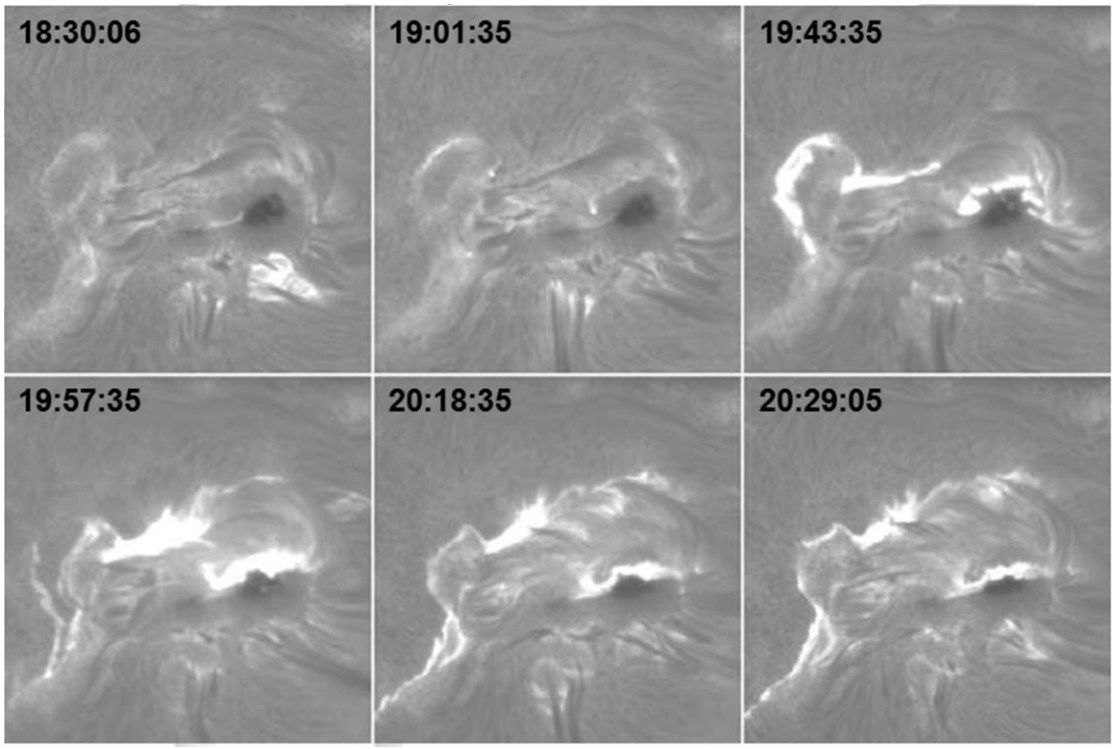

Figure 2. Solar Flare in H-alpha Showing Flare Ribbons. These images were observed from Big Bear Solar Observatory on 29 April 1998. Parallel ribbons, best manifest on the lower-left frame, separate regions of opposite magnetic polarity in the chromosphere. Images adapted from Lang (2009).

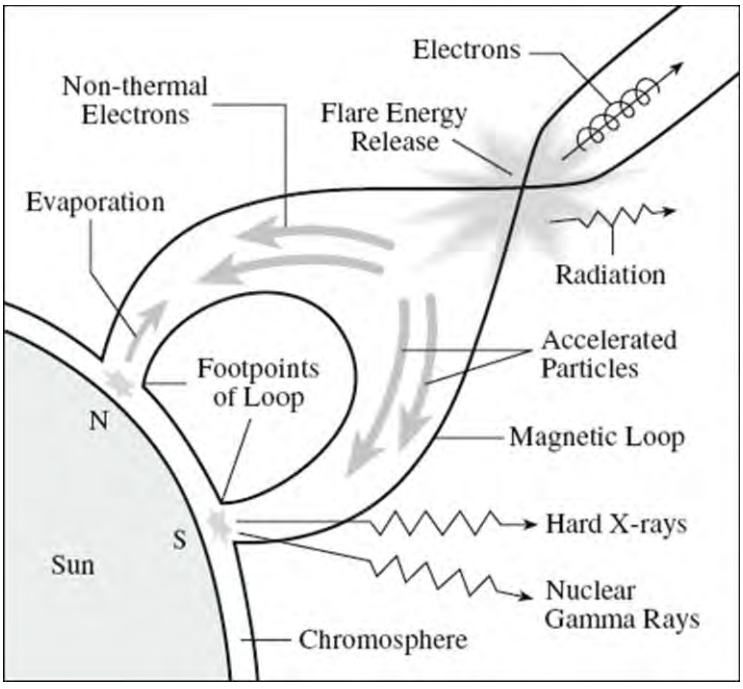

Figure 3. Standard Flare Model. From Lang, 2009.

reconnected magnetic flux loops. As the flare progresses, these footpoints move apart at a speed approximately 15 km/s (Lang, 2009).

When classifying a flare in the H-alpha wavelength, there are two components that are included, importance and brightness. Flare importance is an area measurement of flare size, expressed in millionths of the solar hemisphere. As shown in Table 1, flare importance ranges from 0 (smallest) to 4 (largest).

Table 1. Flare Importance

Importance Category	Flare Area (millionths)
0 (subflare)	≥ 10 to < 100
1	≥ 100 to < 250
2	≥ 250 to < 600
3	≥ 600 to < 1200
4	≥ 1200

Along with the importance factor is affixed a brightness rating divided into three categories: faint, normal, and brilliant. Flare brightness can be defined in a couple of different ways. One way is based upon the amount of visibility on either side of the H-alpha wavelength emission line. For example, a faint (F) flare is distinctly visible as an enhanced area over a line width of 0.8 Angstrom or greater, but less than 1.2 Angstroms. In a normal (N) flare, the flaring area is distinctly visible as an enhanced area over a line width of 1.2 Angstroms or greater, but less than 1.0 Angstrom in either wing. Finally, a

brilliant (B) flare is distinct at 1.0 Angstrom off line center in either the red or blue wing (AFWA, 2010).

The second way define the categories of flare brightness, and the method utilized in this project, is by comparing the brightest point in the flare to the surrounding quiet sun background. In this system, if a flaring region reaches a brightness of 1.6 times (160%) the surrounding quiet sun background brightness, then it is considered a faint (F) flare. There is also a stipulation that the size of the flare brightness subtend an area of at least 10 millionths. For example, to be considered a 'brilliant' flare, the portion of the flare with an intensity of 360% the background brightness must cover at least 10 millionths of the solar hemisphere. The H-alpha flare intensity categories are outlined in Table 2.

Table 2. Flare Intensity

Brightness Category	Percent of Background
Faint	≥ 160% to < 270%
Normal	≥ 270% to < 360%
Brilliant	≥ 360%

Finally, to classify an optical flare according to H-alpha image data, one simply combines the importance and brightness. For example, the least significant classification for a flare is 0F and the most significant is 4B. According to AFWA's manual 15-1, *Solar Environmental Observations*, an 'event-level' solar flare, any at least 2B or larger/brighter, is one that requires heightened awareness and more expedient reporting

and warning procedures due to their possible threat to operations. Because of their importance, event-level flares are given extra consideration in this report. (AFWA, 2010)

2.2.2 X-ray Flare Characterization

Aside from using H-alpha light, another manner in which flares are classified is by the amount of soft X-ray flux (in wavelengths of 0.1 to 0.8 nm) as detected by the GOES geostationary satellites. The X-ray flares are given a letter designation that from weakest to strongest goes A, B, C, M, and X. Each one has a peak flux 10 times stronger than the preceding one. A given letter, or class, has nine subdivisions with each sequentially stronger than the one before. For example, an M2 flare is twice as strong as an M1 flare, while an M7 flare is seven times as strong as an M1 flare. For the details of the X-ray classifications see Table 3 (Lang, 2009).

Table 3. Flare X-ray Classification

Class	Peak soft X-ray flux ($W\ m^{-2}$)
A	Less than 10^{-7}
B	$10^{-7} - 10^{-6}$
C	$10^{-6} - 10^{-5}$
M	$10^{-5} - 10^{-4}$
X	Greater than 10^{-4}

Although for the purposes of this project, flare comparison is conducted in H-alpha light, it is often useful to know both the X-ray and the H-alpha classifications if both exist.

One of the benefits of the X-ray classification is that it is accomplished via satellite and issues caused by the atmosphere and weather are absent.

2.2.3 Flare Phases

Before reviewing the physical processes that trigger a flare, it is instructive to examine how flares release energy as a function of time. From the H-alpha perspective, there are three main flare phases: the preflare phase, the flash phase, and the decay phase. In other wavelengths the phases are similar except the flash phase is typically called the 'impulsive' phase (Figure 4). In the preflare phase there is a gradual increase in X-rays and extreme ultraviolet radiation. This is because the coronal plasma is gradually being heated as magnetic reconnection becomes nearer to being realized. Magnetic reconnection will be discussed in greater detail later in the following subsection. In the impulsive phase (3 to 10 minutes), as this reconnection takes place, electrons and ions with large energies are accelerated and released. While some of these particles are ejected upward, and some are ejected downward back down along the magnetic lines into the chromosphere and can form hard X-rays and Gamma rays as they impact the footpoints in the denser chromosphere. The flash phase (5 to 20 minutes) is accompanied by a rapid increase in H-alpha emissions as the chromosphere is heated and expanded at the footpoints. During this phase, upward motion fills newly formed magnetic loops, causing an increase in soft X-rays (Benz, 2008). Finally, the decay phase is a gradual decrease in flux across all the wavelengths. The shortest wavelengths have already returned to their background state before the gradual decay phase, but the remaining wavelengths (EUV, soft X-ray, H-alpha) show a slow decay for most of an hour or longer, depending on the flare intensity.

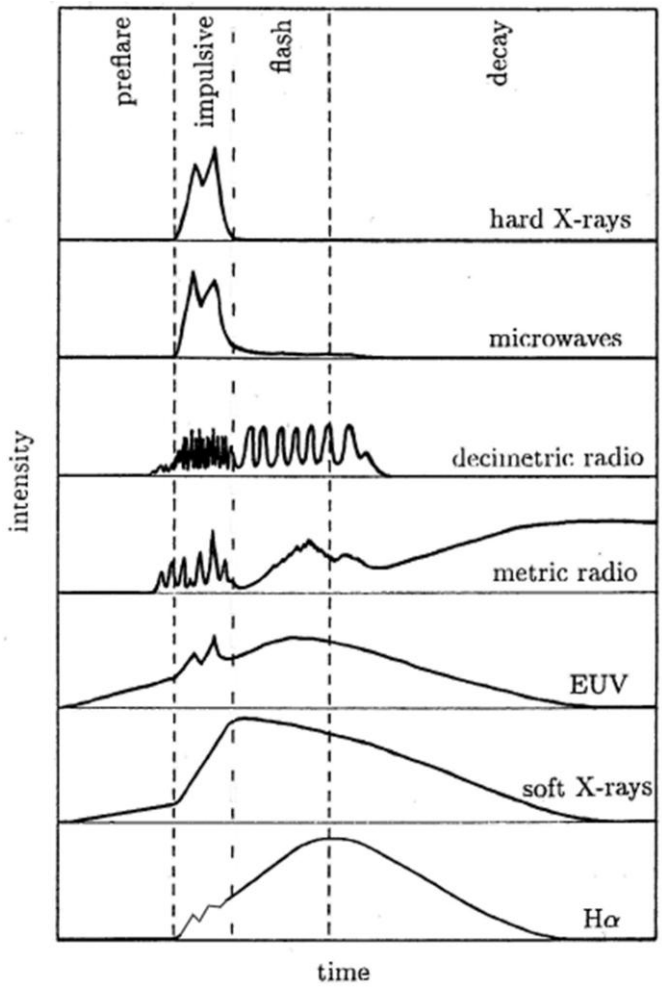

Figure 4. Solar Flare Phases at Several Wavelengths. Adapted from Benz (2008).

An example of flare phases in H-alpha is shown below in Figure 5, where the intensity curve through time is depicted. Figure 5 also shows the corresponding H-alpha flare area progression, which follows a similar trend to the intensity curve. The preflare phase is not always observed in H-alpha, but may be seen in Figure 5 where there is a gradual increase in brightness is noted in the minutes prior to 9:35 UT. The flash phase commences at the left-most vertical dashed line. At this time it is only a matter of minutes before peak intensity and area are noted. The gradual phase, also outlined with

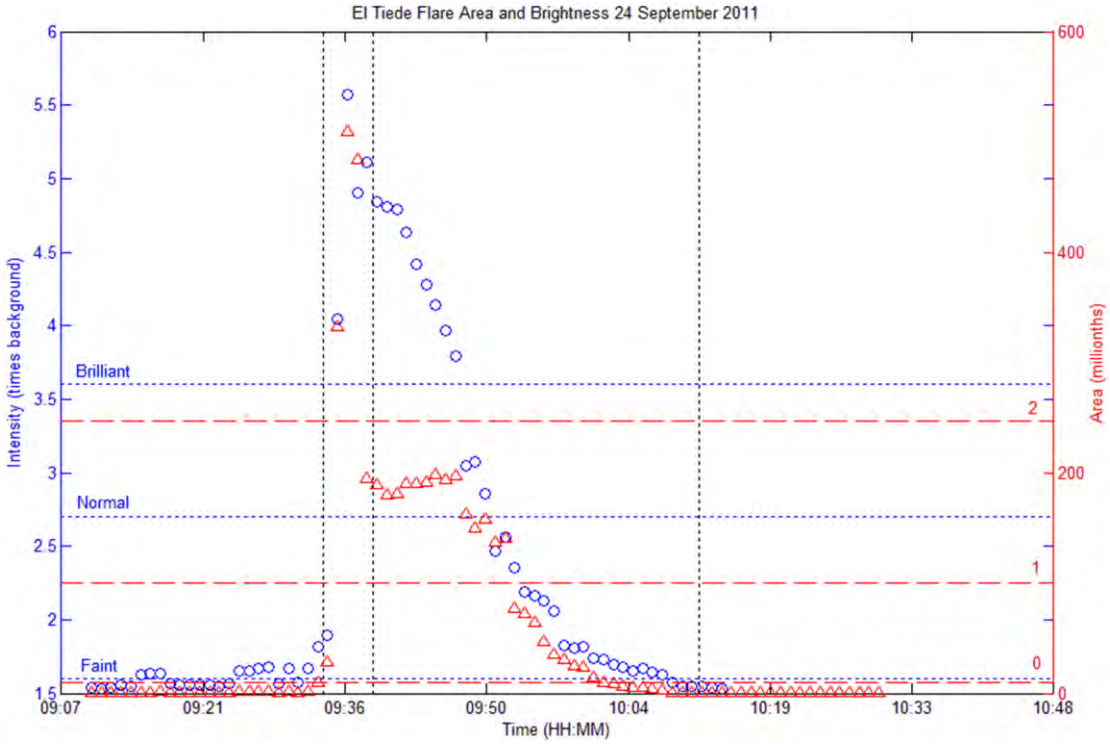

Figure 5. H-alpha Flash and Gradual Phases. This flare was observed at the El Tiede, Canary Islands, GONG site on 24 September 2011. The flare intensity, on the left vertical axis, is in blue and is represented by the plotted circles. The intensity categories listed on the left, correspond to the horizontal lines with small blue dashes. The flare area, on the right vertical axis, is in red and is represented by the plotted triangles. The area categories, listed on the right, correspond to the horizontal lines with large red dashes. The flash and gradual phases are bound by the vertical dashed lines.

vertical dashed lines, lasts for roughly the next hour as area and brightness fall below minimum thresholds in under an hour. Figure 6 shows the GOES X-ray flux associated with the same flare and this time the preflare phase is also outlined on the plot along with the impulsive and gradual decay phases.

2.2.4 Magnetic Reconnection

The process that is thought to trigger solar flares is magnetic reconnection. In the solar corona where such reconnection takes place, magnetic fields are highly

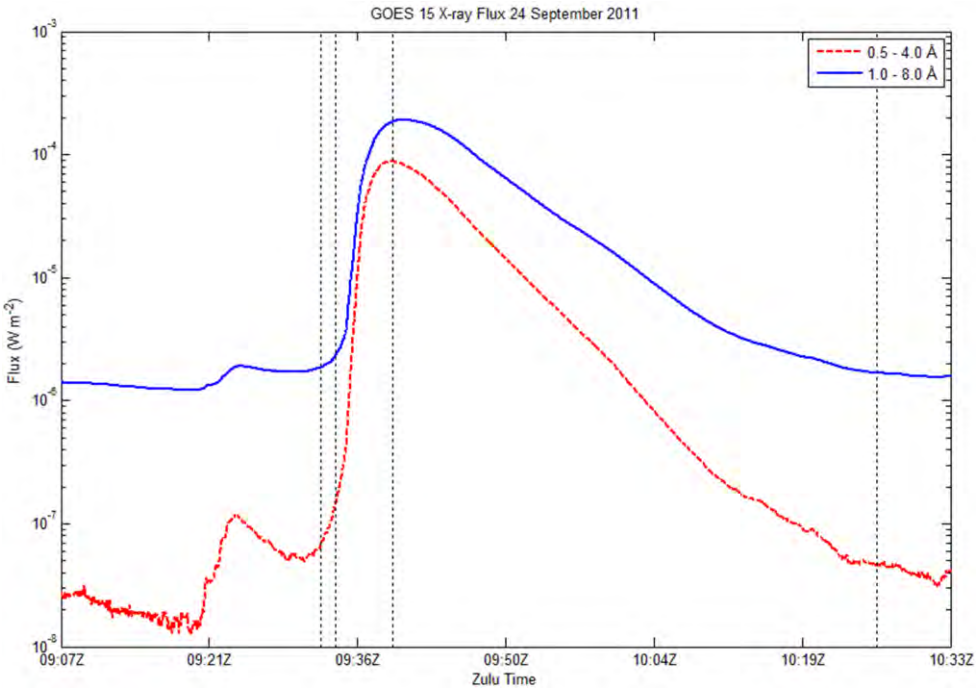

Figure 6. X-ray Flare Phases. This flare was the same flare on 24 September 2011, this time observed with the GOES-15 X-ray Sensor. The solid blue line is represented by the flux at 1.0 to 8.0 Å and the dashed red line is represented by the flux at 0.5 to 4.0 Å. Here the preflare, impulsive, and gradual phases are bound by the vertical dashed lines. Note the slight delay of the longer wavelength X-rays that is commonly observed.

variable in strength and orientation. The solar dynamo constantly generates new magnetic flux that rises from the convection cells and through the photosphere and chromosphere into the corona. Differential rotation combined with convective flows beneath the photosphere causes magnetic fields in the corona to become increasingly twisted and complex. This magnetic stress continuously builds up over time. The process that relieves this stress is referred to as magnetic reconnection, a process that releases the magnetic energy that has built up due to complex flows below. Typically reconnection takes place suddenly and violently—hence the released energy is manifested in solar flares (Aschwanden, 2005).

The process of magnetic reconnection allows magnetic energy to be dissipated in the form of heating of the local plasma. As mentioned above, the solar dynamo is constantly producing areas of enhanced magnetic flux that have finite life cycles. This means new magnetic flux propagating upwards from the interior regions will encounter pre-existing magnetic flux in the corona.

This is similar to a perhaps more familiar scenario when the solar wind encounters the Earth's magnetopause and the bow shock is formed. In the corona where the flux systems interact there will be a boundary that forms where the magnetic fields are pointing in opposite directions on either side (Figure 7). For this example, assume that these fields point in the east/west directions as viewed from above the solar surface. At the boundary between the magnetic regions, the local magnetic field drops to zero to

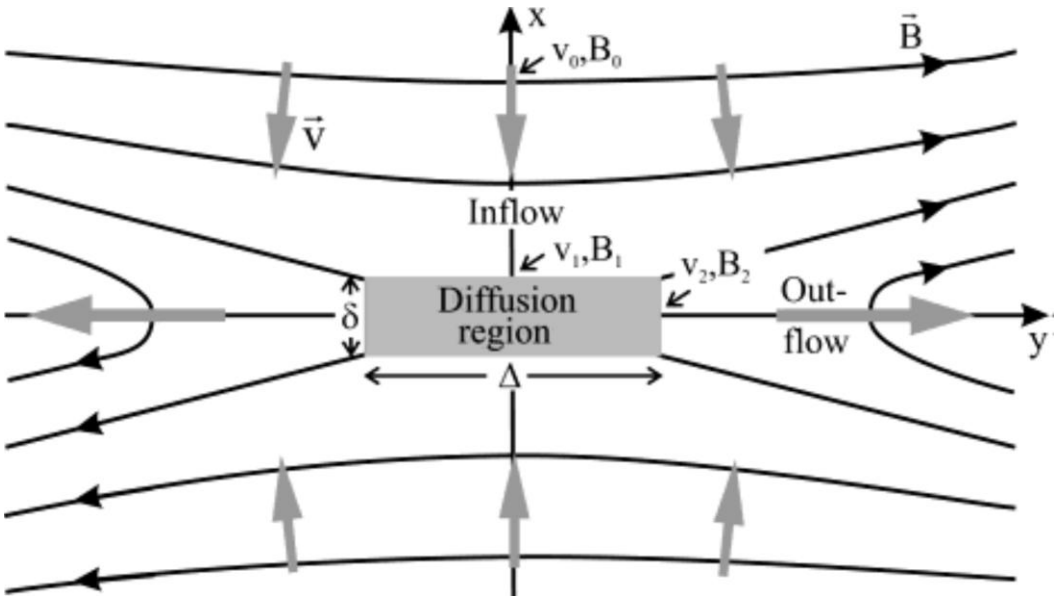

Figure 7. Two Dimensional Magnetic Reconnection Model. Adapted from Aschwanden (2005).

balance the boundary conditions on either side. Recalling Ampere's law, this implies the presence of a vertical current sheet that forms in the region of no magnetic field. In this transition region there must also be an increase in the thermal gas pressure. The equation for balance between magnetic and thermal pressure is given by Aschwanden (2005):

$$P_1 + \frac{B_1}{2\mu_0} = P_2 + \frac{B_2}{2\mu_0} \tag{2.1}$$

In this case if B_2, the magnetic field in the neutral boundary layer, is nearly equal to zero, the value for P_2 must compensate by increasing. This region where the two oppositely directed magnetic flux systems approach is finite (i.e. the magnetic neutral line extends only so far east and west), and on either side of this region, at the ends of the neutral boundary line, the increased thermal pressure is able to be relieved. In this region there are outflows and in the region where the magnetic flux systems are directed in opposite directions (i.e. from the north and south) there are inflows. The central boundary layer where the magnetic field is weak is often called the diffusion region and is the point plasma is redirected from the inflow region to the outflow region (Figure 7). If these processes of magnetic reconnection are able to happen quickly enough, plasma particle acceleration to relativistic velocities takes place in the form of a solar flare. This two dimensional example is highly idealized. There are many three dimensional models that have been developed that attempt to model a 3-D flare more closely. The usefulness of the two dimensional model is its simplicity and general principles which in reality are more complicated but basically are followed (Aschwanden 2005).

Many scientists have contributed to the standard flare model, but the primary authors are recognized to be Carmichael (1964), Sturrock (1966), Hirayama (1974), and

finally Kopp & Pneuman (1976). This is why the standard flare model is sometimes called the CSHKP model. The standard flare model is a basic approximation, and there are still many studies that are involved in deducing the details of the process (Shibata, 1998). A visual depiction of the standard flare model, is given in Figure 3 earlier in the chapter.

As was discussed, the first stage in the standard flare model is the magnetic reconnection. Typically this reconnection occurs at the top of a magnetic loop near magnetic field lines of opposite orientation. As the reconnection takes place electrons are accelerated to high speeds though different processes. Although these processes are not well understood it is thought that the free magnetic energy combined with the electric current sheet and field are responsible for generating the shock waves as the flare takes place (Benz, 2008). As the particles are accelerated to high speeds impulsive radio waves are generated as well as a burst of hard X-ray emission at the loop top. Non-thermal electrons may be accelerated away from the solar surface while continuing to produce waves, or may travel down the newly formed loop lines and impact the denser chromosphere at near relativistic speeds. This impact takes place at the loop footpoints which have opposite magnetic polarity. Here they emit more hard X-rays due to electron-ion bremsstrahlung radiation. Some accelerated protons impact the footpoints with such high energies that they are able to emit gamma rays. Because chromospheric material is heated so quickly, electrons with lesser energy propagate mostly upwards along the magnetic loops, emitting soft X-ray radiation through a process called chromospheric evaporation. Chromospheric evaporation is a manifestation of the decay phase of a flare (Lang, 2009).

Of interest for this project is the temporal correlation between the H-alpha flare and the hard X-ray peak. Such findings suggest that the H-alpha flare is a manifestation of the initially accelerated high energy, non-thermal electrons that impact at the footpoints. (Kurokawa, 1988) In the chromosphere, the ambient Hydrogen that has been ionized and recombined emits a photon as it decays from the n=3 state to the n=2 state. Temmer et al. (2001) reported the statistics regarding H-alpha flares, considering a total of 100,000 flares in H-alpha between 1975 and 1999 that covered two complete solar cycles and portions of a third. They found that the rise and decay times on average increase with increasing importance class (area). The increase is more pronounced for the decay times than for the rise times. The same trend is noted for flares of greater brightness though not as significantly. In 90% of H-alpha flares the decay time was longer than the rise time. For more than half of flares, the decay time was at least four times as long as the rise time. On average the event asymmetries increase with the importance class. Additionally the study found that the duration varies as the solar cycle varies. In other words longer flares were most predominant during the solar maximum period and shorter flares most likely to be found during solar minimum. This is due only to the difference in decay times since the rise times of flares were not found to have a significant correlation with the solar cycle. In fact the decay time during solar maximum was found to last on average 1.5 times longer than the decay time during solar minimum. The results suggest that temporally, the cooling phase of the flare in H-alpha is more strongly affected by changes in the chromospheric plasma than the rising phase is (Temmer, 2001).

2.3 Solar Observing Optical Network H-alpha Data

The Solar Observing Optical Network (SOON) is currently the Air Force's primary means for monitoring solar active regions at optical wavelengths. SOON consists of three solar observatories distributed longitudinally—in New Mexico, Australia, and Italy—to maintain continuous solar coverage throughout a 24 hour day (Figure 8).

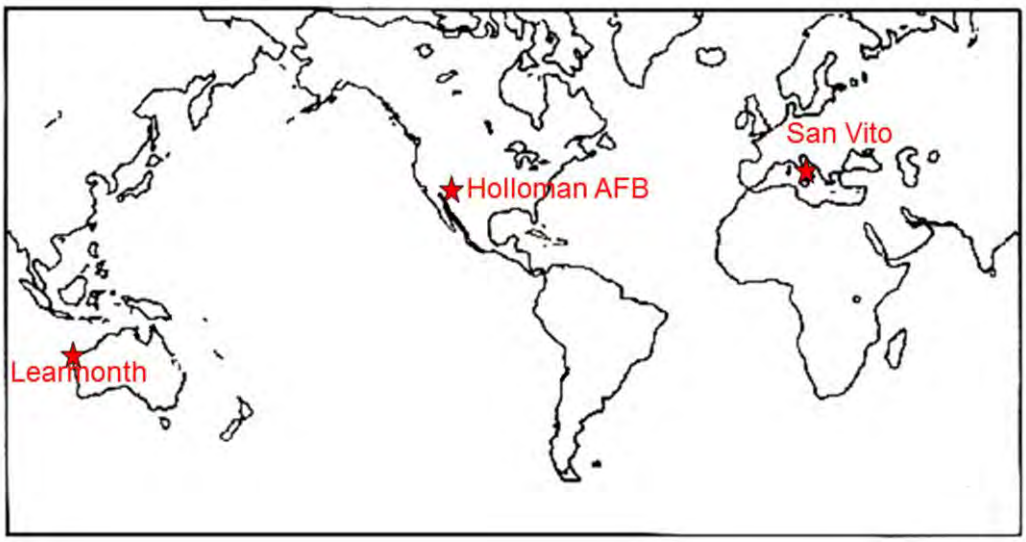

Figure 8. Worldwide distribution of SOON observatories.

The principal telescope is a 25-centimeter evacuated refractor mounted on a polar axis for solar tracking (Figure 9). The primary observation tool for solar flare measurements is the tunable optical filter centered on the H-alpha absorption line where the flare shows most brightly in the visible wavelengths. Observations are typically made through the video system in which a camera converts the optical H-alpha image into analog video. Next the analog video is converted into electrical signals for measurement.

Figure 9. Primary telescope at the SOON site at Holloman AFB, New Mexico. Image courtesy of the Holloman observatory.

An instrument called a videometer uses these signals as input from which it calculates a brightness and area of flares every 30 seconds for the automatic reporting. The observer may choose to tune the filter slightly off center from the H-alpha peak, which results in pictures of the solar surface region at differing depths. The videometer clock is ensured to be within one second of a Coordinated Universal Time (UT) source. As outlined in Air Force Weather Agency Manual 15-1, a clock accuracy check is performed at least once daily when the observatory opens for the day.

During flare patrol, the observer defines pre-set rectangular regions centered on numbered active regions on the solar surface. Although the resolution of the telescope eyepiece is 0.67 arcseconds in large scale mode (for the active regions) and 2.88 arcseconds in full disk mode, some of this resolution is lost as the visible light is converted to a digital image. The effective resolution of the system after the analog to

digital conversion process is about 2 arcseconds in large scale mode and about 10 arcseconds in full disk mode. For reference, each of the six frames in Figure 2 is 300 arcseconds in width, or about one sixth of the angular extent of the sun.

The videometer scans these 'targeted' active regions and determines the amount of solar surface area that is of certain brightness levels. The 6 bit accuracy system contains 64 brightness levels or bins, which will be discussed further in the third chapter. By using these data, quantitative measures of flares are determined, including growth and decay rates, and precise area calculations (ARINC, 2006).

The SOON imagery archival system is called the Digital Image Processing System (DIPS). The analog output from the video camera mentioned above is also inputted into DIPS which converts the analog signal into an 8-bit digital image with 256 possible levels of brightness for each pixel. The image size stored by DIPS is an array of 512 by 512 pixels and may show the entire solar disk or a regional portion of the sun of higher resolution. The images are stored in the Flexible Image Transport System (FITS) format which include not only the image array of the solar disk itself but also a header accompanying each image with background information about the configuration of the image, camera, and telescope (ARINC, 2006).

2.4 Global Oscillation Network Group H-alpha Data

The Global Oscillation Network Group (GONG) is a global network of observatories operated by the National Solar Observatory that are located strategically in favorable locations for viewing the sun. The primary mission of GONG is in the field of helioseismology, however recently the capability for imaging solar flares in H-alpha has

been added to GONG. The six observing sites of the GONG network are located in California, Hawaii, Australia, India, the Canary Islands, and Chile (Figure 10). With these six observing sites, GONG has the capability to observe the sun from two or sometimes even three locations at the same time. In such a case, each site provides an H-alpha image twenty seconds before or after adjacent sites to the west or east, respectively. Thus the maximum possible time resolution is an image every 20 seconds. The time-stamps on GONG images utilized in this project are expressed in UT, and are accurate to better than a microsecond thanks to GPS receivers at each observatory.

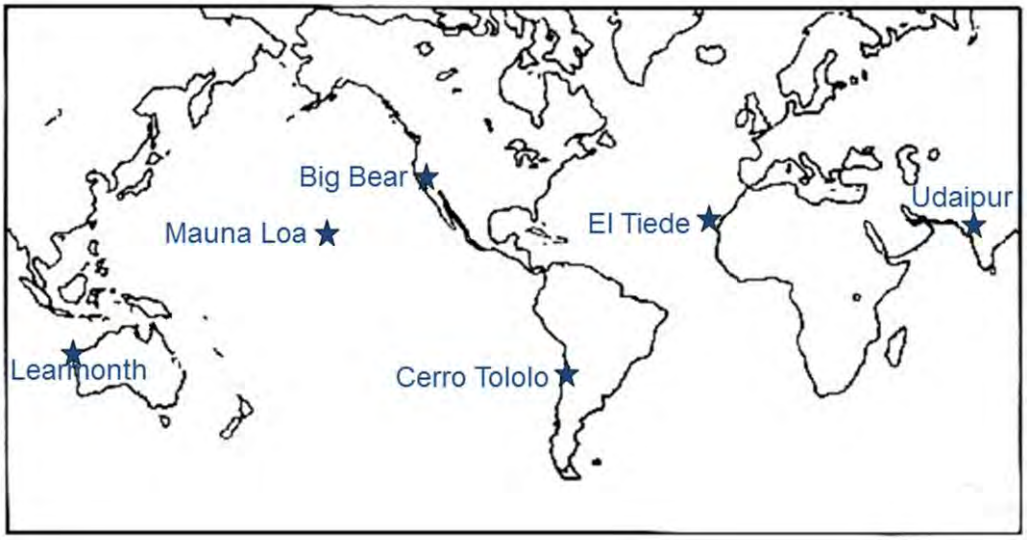

Figure 10. Worldwide distribution of GONG observatories.

The design of the GONG H-alpha imaging system begins as visible light is captured by a 7-inch primary lens, then encounters a beam splitter. The beam splitter allows the light that is near the H-alpha wavelength to be isolated and further processed later. After passing through some reimaging optics the light passes through a 0.4 Å bandpass filter. This further narrows the H-alpha light even more precisely to the

wavelength of 6562.8 Å. The precision of the filter allows for better contrast when viewing flare and other features in the chromospheric disk (Lang, 2009). Finally after passing through the focusing lens the image is captured by the CCD camera with resolution of 2048 x 2048 pixels. Because the H-alpha camera has its own dedicated data acquisition system (separate from the other GONG systems) it is able to transmit imagery to the Air Force Weather Agency within one minute of imaging, and enables nearly real-time analysis by dedicated observers (Hill et al., 2009). Figure 11 shows the GONG site at Learmonth, Australia.

Similar to the SOON system, GONG images are stored in FITS format. The full disk image of the H-alpha sun is fitted to the center of the aforementioned 2048 by 2048 array, and exposure times are automatically adjusted to maintain the quiet disk center at 20% dynamic range (the range of luminosity that can be accurately captured by the detector). This establishes a baseline quiet sun background and prevents saturation by bright flares. The CCD camera in the GONG system utilizes a 16-bit analog to digital converter, so there are over 65,500 possible brightness values. H-alpha measurements from GONG are interpolated such that the solar disk is made to have a fixed diameter of 1800 pixels in both the x-dimension and the y-dimension. This produces solar images with a resolution of about two arc seconds, though variations in atmospheric seeing conditions sometimes degrade this to a lower resolution (Harvey et al., 2011).

Figure 11. GONG observatory at Learmonth, Australia. The exterior portion of the telescope is noted on the near short side of the shelter. http://gong.nso.edu/instrument/

3. Methodology

3.1 Chapter Overview

This chapter describes the methods that were used to perform this research. The first section addresses the method of data collection for the project. Next, the methods used to analyze the data are discussed.

3.2 Data Collection

Data collection for the project consisted of obtaining flare observation alphanumeric text messages from the three SOON observatories in order to get the most detailed information regarding the observed flare characteristics. Archived solar H-alpha data was also obtained directly from the SOON observatories, and from the GONG sites via FTP.

3.2.1 SOON Flare Text Bulletins

One of the first objectives in initializing the project was to obtain the text (ascii formatted) data from the SOON sites. The text bulletins that are of particular interest are the solar flare alerts issued by the observatories to report optical solar flares as viewed in H-alpha. These reports are quality controlled by the observer on duty and include flare brightness and area rating, and several other useful elements. The flare brightness describes how bright the flare was compared to the background, expressed as a two digit number. For instance, a normal flare could have a brightness level of 3.1 times the background brightness. Flare brightness is given in bin levels above a background level. Typically the minimum threshold for a faint flare is the 16^{th} brightness bin, which is an intensity of 1.6 times the background brightness, however this can be nudged upwards as

the observer deems necessary. For example, if an active region contains a large amount of plage, it may trigger a false flare alarm if it exceeds a brightness of over 1.6 times the local background brightness. Plage brightenings may last for several days, so an observer may choose to set the flare threshold to such a region at 1.7 or 1.8 times the background level, as is outlined in the Air Force Weather Agency Manual 15-1 (AFWA, 2010). The flare brightness must not only surpass the minimum threshold of 1.6, but this brightness must also cover an area of at least 10 millionths corrected area. This corrected area is another piece of information that is included in these bulletins. The corrected flare area is expressed in whole millionths of the solar hemisphere. This area, calculated at the time of maximum brightness, is the value that determines the overall importance class on the scale from 0 to 4 (see Table 1). Some of the other parameters reported in these text bulletins are: flare start, peak, and end times (reported in whole minute increments), and the location and region number associated with the flare. If a flare observation is degraded for any reason, such as clouds, or proximity to sunrise or sunset, then the observer appends a plain language note of this at the end of the text message. There is also an observation quality that is noted in the message expressed on a scale from 1 to 5, with one being very poor conditions and 5 being excellent conditions. The default level is 3, or fair. Figure 12 contains a sample text bulletin with examples of many of the elements explained. Further details regarding the flare text bulletins are contained in Air Force Manual 15-124, *Meteorological Codes*.

3.2.2 SOON Text Bulletins Compared to GONG Image Analyses

After obtaining archived H-alpha imagery from the SOON observatories some significant limitations were realized. The primary disadvantage of the digital imagery from the

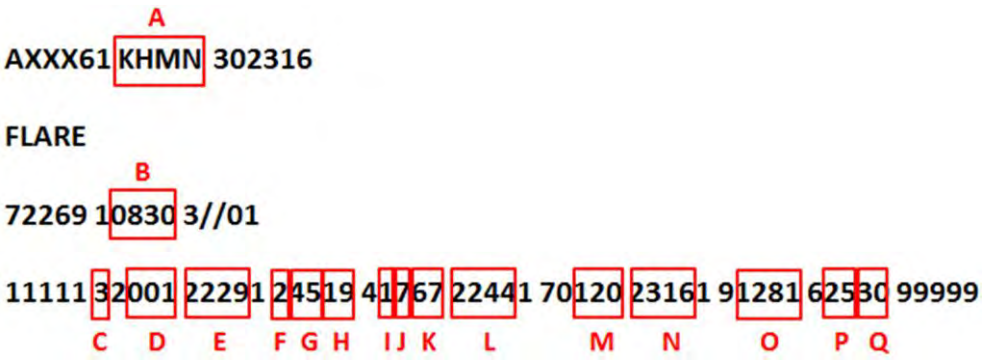

Letter	Explanation	Letter	Explanation
A	Site = Holloman, AFB, NM Observatory	**J**	Brightness category = 7 = faint
B	Month & Day = Aug. 30	**K**	Characteristics = 6 = one or more brilliant points 7 = high speed or dark surge on disk
C	Observation quality = 3 = fair	**L**	Peak time = 22:44 UT
D	Local flare serial number = 1 = 1st flare of the day	**M**	Corrected area at time of max brightness = 120 millionths of hemisphere
E	Start time = 22:29 UT	**N**	End time = 23:16 UT
F	Solar quadrant = 2 = southeast	**O**	SWPC region number = 1281
G	Central Meridian Distance = 45 degrees	**P**	Peak flare brightness (bin value) = 25 = intensity 2.5 times background (minimum 10 millionths area)
H	Latitude = 19 degrees	**Q**	Peak flare brightness (bin value) = 30 = intensity 3.0 times background (no minimum size requirement)
I	Area category = 1		

Figure 12. Sample SOON Flare Text Bulletin. From Holloman Observatory on 8 August 2011.

DIPS system is that it is not calibrated for flare analysis (unlike the videometer, see Section 2.3). Although the background sun may be at a relatively constant brightness level, based on the author's analysis of DIPS imagery, most flares saturate the pixels at

the brightest possible pixel value (256^{th}), meaning the true brightness of the flare is not being captured in the image. Because area calculation depends on brightness, it is also adversely affected. Additionally, on some DIPS imagery there are artificial image distortions, such as dark horizontal lines that appear across the surface of the solar disk. Because it is such an old system, it is not constantly in good working order; there are frequent times where DIPS is not operational and archived imagery is not available (Kennewell, 1998). Missing data due to system outage and degraded data was encountered by the author while collecting DIPS imagery from the observatories during the period of this study. While DIPS is an effective tool for general viewing of flares after occurrence, it is unsuitable for scientific analysis. Because DIPS imagery does not accurately capture flare brightness and area, ultimately it was decided not to analyze this imagery from the SOON observatories for this project, but instead to rely on the corresponding flare text bulletins for comparison with analysis of imagery from the GONG system.

Thus the flare text bulletins became the source of flare classification from the SOON observatories and based on these bulletins, the number and type of flares observed was tabulated. The total number of H-alpha flares reflected by the SOON text bulletins during the period of study follows in Table 4. The vast majority of these flares are of the smallest kind, and this is expected based upon statistical analyses of H-alpha flares, notably in Temmer (2001). In this survey, Temmer analyzed over ten thousand flares from 1975 to 1999, the importance category of 0 consisted of roughly 90% of total flares, the importance category of 1 consisted of about 9% and importance category of 2 consisted of about 1% of flares. Although the total number of flares considered in this

Table 4. Total SOON Flare Count for fhe Time Period of this Research Project

Importance \ Brightness	Faint	Normal	Brilliant	Total	Percent
0	900	12	0	912	91.2
1	44	24	4	72	7.2
2	1	6	8	15	1.5
3	0	0	1	1	0.1
4	0	0	0	0	0.0
Total	945	42	13		
Percent	94.5	4.2	1.3		

project is only 10% of the numbers surveyed by Temmer, the relative percentages of each of the flare categories are similar.

GONG imagery for the flares listed in Table 4 was downloaded, when possible, for comparative analysis. Since SOON text bulletins contain flare start and end times, in each flare case GONG imagery for these times was collected in addition to imagery of at least 10 minutes before the SOON start time and 10 minutes after the SOON end time. One-minute GONG imagery (per site) corresponding to all of the flares larger or brighter than 0F (subflare) was collected, in addition to imagery corresponding to all flares that were observed by two SOON sites, regardless of flare size. For example, on 3 August 2011, the SOON observatory at San Vito, Italy reported an H-alpha flare starting at 13:20 UT, with a flare peak time of 13:50 UT, and a flare end time of 15:38 UT. This flare was observed by GONG sites at Cerro Tololo, Chile, and El Tiede, Canary Islands. A total of

315 FITS images were downloaded and processed for this event. The average number of images per event was 162, the smallest number was 29, and the largest event included the analysis of 887 images. There were some flares where GONG imagery was either partially or fully available online due to unknown reasons (weather, maintenance, data outages, etc.). Where significant portions of flare evolution were missing especially near flare peak time (based on information from SOON bulletins), a flare categorization could not be made, and these cases were discarded. The results of comparisons within SOON and GONG and between SOON and GONG are contained in Chapter. 4.

3.3 Data Analysis

This section of the report contains a description of the methods by which imagery was analyzed for this project. The first subsection (3.3.1) includes background information on the development of the computer program code used. The second subsection describes how flare brightness was calculated within the code, followed by the third and fourth subsections detailing the methods by which flare area and sharpness were analyzed, respectively. Finally is an example of the step-by-step procedure of actually running the code to analyze a specific flare. The examples outlined in the following subsections apply to GONG imagery since SOON imagery was not utilized for this project (see Section 3.2.2).

3.3.1 Development of Code for Analysis

In order to analyze the solar imagery, a program was needed to read in the FITS files and characterize brightness and area qualities. Fortunately, there is a preexisting software package called SWIFT, which has been developed to analyze solar H-alpha

imagery. The acronym SWIFT is from the term SWFL/ISOON Flarecast Tool. SWIFT was originally developed by the Air Force Research Laboratory's Space Weather Forecasting Laboratory (SWFL) for the Improved Solar Observing Optical Network (ISOON), the next generation observing system intended to replace the current SOON system. Since that time, a modified version of SWIFT has been developed to be able to analyze GONG H-alpha data (Henney, 2011). The software is written in Interactive Data Language (IDL) and may run on a number of different platforms. SWIFT is configured to perform real-time flare detection in IDL through a graphical user interface. This posed a problem for the current project, as archived imagery is not able to be analyzed in the current SWIFT configuration. For example, the program is designed specifically to operate by utilizing the computer system time and requires imagery to be within a certain window of time near the system time. Also it requires the user to be connected to the internet so it can access other time-sensitive information such as SWPC solar active region information. The complex structure of over 300 interdependent source code scripts in SWIFT could not be easily manipulated to resolve these issues.

In order to overcome this, new code was written to perform analysis on the downloaded GONG imagery. An additional primary script was written to characterize flare brightness and area, and an additional routine was added to compute sharpness. Both analyze a time sequence of FITS images. The new code did utilize nine of the original source code scripts from the SWIFT library, which mainly performed the function of reading FITS images and header information. The methods by which flare brightness, area, and sharpness were calculated are addressed in the following three subsections.

3.3.2 Brightness Computation

In order to characterize a flare, one needs to know how bright the flare is compared to the surrounding quiet background. After this is accomplished, the size of the flaring (bright) region can be measured and flare category ratings assigned. The GONG FITS images to be analyzed include a full disk H-alpha image of the sun contained within a 2048 by 2048 pixel array, with the diameter of the sun of 1800 pixels. Each element of the array represents a brightness value, and IDL reads these values in order to determine the flare intensity.

Once a peak brightness pixel value has been established (within a sub area containing a flaring region), it is compared with the local background. In order to establish a sufficient quiet-sun background, a box around the flare is defined that is centered on the flare but includes a sufficient sampling of background conditions. According to AFWA's manual 15-1, SOON observatories require that box sizes be a minimum of 150 by 150 arcseconds, which equals approximately 150 by 150 pixels in GONG imagery (AFWA, 2010). The primary concern with the box size is to have enough of a sampling of the background solar intensity so the background level can be determined. For this project, a box size of 400 by 400 pixels was a sufficient sampling of the local background, although for flares near the limb the box size is smaller to avoid sampling 'dark' areas on or beyond the limb. If the box size is too small and only the flare included within it, the algorithm may mistake flaring region for the background region since there may be more flaring pixels than background pixels in the box. Figure 13 shows an example of a full disk GONG image and a typical 400 by 400 pixel box used to sample the local background.

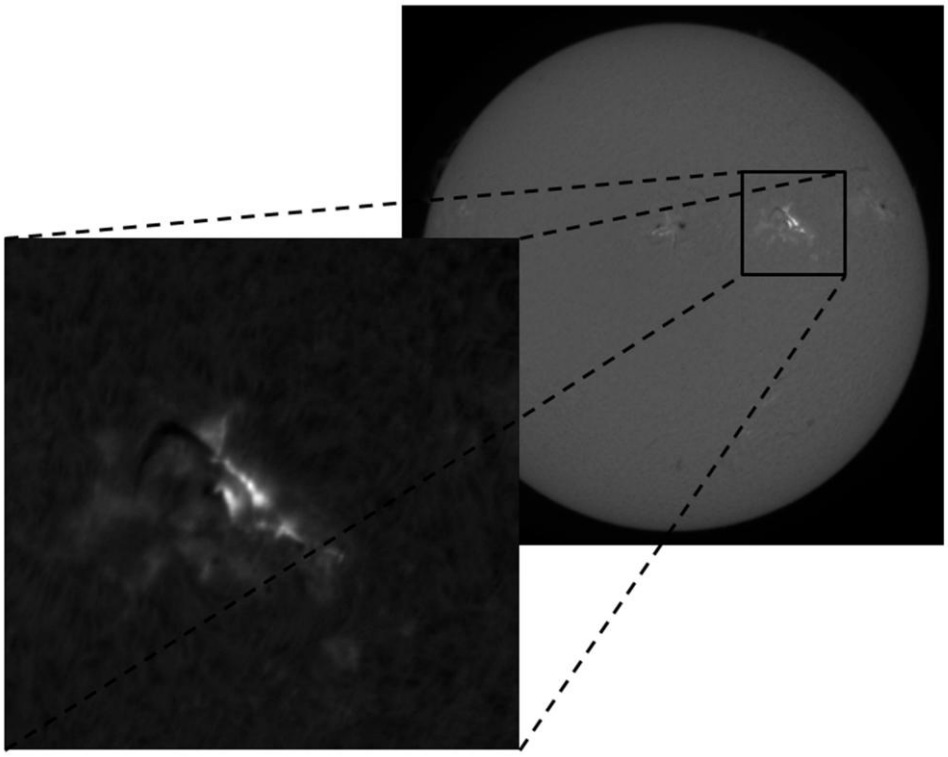

Figure 13. Full disk GONG image and 400 by 400 pixel sub area. From Cerro Tololo, Chile GONG Observatory on 3 August 2011 at 13:34 UT, the time of flare peak brightness.

Next, the brightness of the regional background is calculated in order to compare it with the peak brightness of the flare. The algorithm accomplishes this by counting the number of pixels in each possible level of brightness within the box, and then determining the peak of the distribution of pixel values. The peak of this distribution is at the intensity value of the local quiet background. Figure 14 shows an example, where the peak of the distribution of pixels is represented by the dotted line. In this case, the brightness value where this peak is located at is 3176. The pixels that have a value of 1.6 times this value, in this case a value of 5082, are considered the flaring pixels and are outlined by the dashed box in Figure 14. The right side of the dashed box contains all of

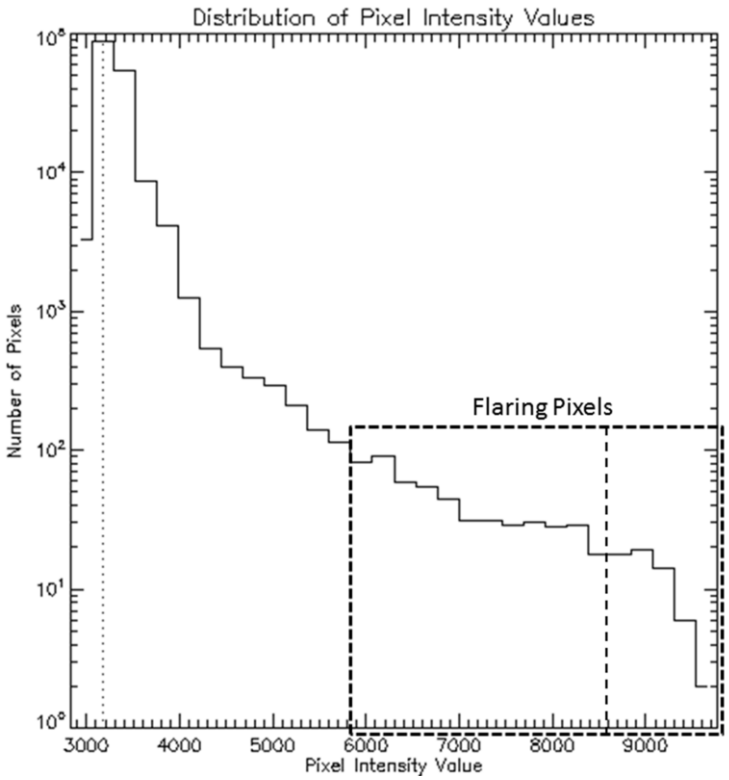

Figure 14. Histogram depicting distribution of pixel intensity. From Cerro Tololo, Chile GONG Observatory on 3 August 2011 at 13:34 UT.

the pixels that have a brightness value above 8575, which is 2.7 times the background value of 3176. Recall that 2.7 is the threshold for a flare of 'normal' brightness. This flare then is considered a 'normal' flare, assuming the corrected area of these pixels was greater than 10 millionths (the minimum classification for area). Discussion on how area is calculated is continued below in the following subsection.

3.3.3 Area Computation

Solar flare area is reported in millionths of the solar hemisphere, termed corrected area. Since the spherical sun is observed as a projected disk on a flat plane, flare area on a disk (apparent or measured area) must be corrected in order to be reported as millionths of the hemisphere. Figure 15 illustrates how a feature (or flare) on the solar disk,

represented by the red spot, will have a decreased apparent area as it approaches the solar limb.

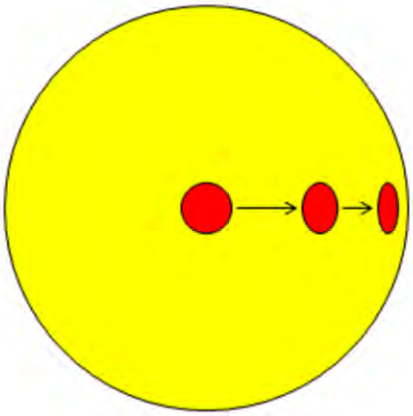

Figure 15. Solar Measured Area vs Corrected Area. The red spot depicted in three different locations contains the same corrected area in all three cases, but the measured (or apparent) area decreases the nearer to the limb it is located. This is because these regions are viewed at a large angle relative to the solar surface normal.

This effect is called geometric foreshortening. A correction is necessary for geometric foreshortening as well as for the vertical height of the flare, which may be thousands of kilometers. The magnitude of these effects (Equation 3.1) increases with increasing distance from the center of the solar disk. This equation is the same correction used by the SOON observatories, and was based on a statistical study of 4700 flare observations at Sacramento Peak Observatory (Smith and Smith, 1963).

In order to apply these corrections, the distance from the center of the disk must be included in the computer algorithm. It is therefore necessary to use the geocentric solar coordinate called the *radius vector* (R_v). The radius vector is a measure of the distance from the center of the observed solar disk to in this case, a solar flare. Flares

that occur on the observed solar disk range between an R_v of zero at the center of the solar disk to an R_v of 1.0 on the limb. Thus the magnitude of R_v can be used to specify how much to correct for geometric foreshortening, with increasing correction corresponding to increasing R_v, below:

$$A_c = \frac{A_m}{0.2R_v + \sqrt{1 - R_v^2}} \tag{3.1}$$

In the equation, A_m represents measured area and A_c for corrected area. The square root factor is the adjustment for geometric foreshortening while the 0.2 factor is the adjustment for flare height. In H-alpha imagery, flaring regions have a vertical extent and thus they appear as being above the chromospheric surface. Because areas are specified in terms of the chromospheric surface, the vertical height correction is applied. As is seen in Equation 3.1, without this adjustment the difference between measured area and corrected area would be even greater. In this equation, measured area and corrected area are expressed in terms of millionths of the solar disk. In order to convert corrected area to be expressed in terms of millionths of the solar hemisphere (as solar flare areas are officially expressed) it is necessary to multiply $0.5 \times A_c$ (Smith and Smith, 1963). This is identical to the method applied by the SOON observatories, as outlined in AFWA's manual 15-1 (AFWA, 2010).

The IDL algorithm used in this project utilizes the same methods outlined above, and computes flare area in GONG imagery as follows. Since the solar disk in GONG has the same apparent radius and area in all archived imagery, it is not difficult to compute measured flaring pixel area. The pixel area in GONG of the entire solar disk is 2.54469×10^6 pixels, based upon the known diameter of 1800 pixels. The measured

flaring area is simply the number of pixels flaring divided by the number pixels in the disk. In the flare example from Cerro Tololo, Chile at 13:34 UT (Section 3.3.2), there were 1115 pixels above the minimum flaring threshold intensity value of 3176. If 1115 is divided by the total number of pixels in the disk (2.54469×10^6), multiplied by 0.5 (to express in hemispheric terms) and converted to millionths, the flare measured (apparent) area is obtained. In the example case the measured area is 219 millionths.

The corrected flare area is accomplished in a similar manner except this time each flaring pixel is given a different scaling (or correction) according to the denominator of Equation 3.1, since each pixel in the GONG imagery has its own R_v value (that stays constant across all GONG imagery). Equation 3.2 shows an example of the scaling for a pixel with an $R_v = 0.5$.

$$Weight = \frac{1}{0.2R_v + \sqrt{1 - R_v^2}} = \frac{1}{0.2(0.5) + \sqrt{1 - 0.5^2}} = 1.035169 \qquad (3.2)$$

Now that each pixel has its own weight, the procedure to calculate area is similar to before, where the weights of all the flaring pixels are totaled, which is divided by the total number of pixels in the disk. In the example, the corrected flare area was calculated to be 228 millionths. One point to note is that the shape of the flare is not accounted for in the area calculation; the algorithm simply accounts for all pixels that are above the threshold and those are counted as flaring. If the flaring region was distributed among four flare ribbons or two flare ribbons they would all be counted as flaring regardless, no matter their distribution in the local region box. According to AFWA's manual 15-1, This is also the case at the SOON sites, where the videometer does not account for the flare shape or distribution (AFWA, 2010).

3.3.4 Sharpness Computation

Brightness and area are the only two characteristics that are routinely used to describe H-alpha flares by the SOON sites. In addition it is critical to know the quality of the atmospheric seeing conditions at the time flare observation as it may be used to gauge the quality of the observation, particularly when seeing conditions are poor. The SOON observatories accomplish this by including the rating the quality of the observation on a scale from 1 to 5, with one being the poorest and 5 the best. This is of limited value, however, since it is a subjective call by the observer, which understandably varies from observer to observer and from site to site (see AFWA's manual 15-1). As an approximate measure of atmospheric seeing conditions, the degree of sharpness of every flare was determined by adding a sharpness algorithm, based on work by Harvey et al. (2011), into the IDL code. First the routine crops a centered 180 by 180 pixel sub image from the box centered on the flaring region (Section 3.3.2) and applies a smoothing function to this image. The smoothing function applies a series of 9 by 9 pixel filter to the original 180 by 180 image. This is accomplished by assigning a value to each pixel in the 180 by 180 sub array based on the average of the center pixel and the eight adjacent pixels.

After a smooth image is established from the original image (each 180 by 180 pixels), original image array is divided by the smoothed image array. The result is a new array of the same dimensions, and the standard deviation of this new array is calculated. The result is the sharpness parameter such that a high value means there was a significant difference between the smoothed image and the original image (favorable atmospheric seeing producing a sharp image of good resolution). A small value of sharpness

parameter means that the original image was already relatively smooth (poor atmospheric seeing conditions, and lesser effective resolution) and thus there was less of a difference between the smoothed image and the original image. An additional factor that affects the sharpness parameter (besides atmospheric conditions) is the degree of uniformity of the H-alpha sun. An image containing different features such as flares, areas of plage, or solar filaments would have a higher sharpness than an image without these features.

Two examples of the original sub image and the smoothed image are shown below Figure 16. The top case is where the original image (left) is fairly sharp and

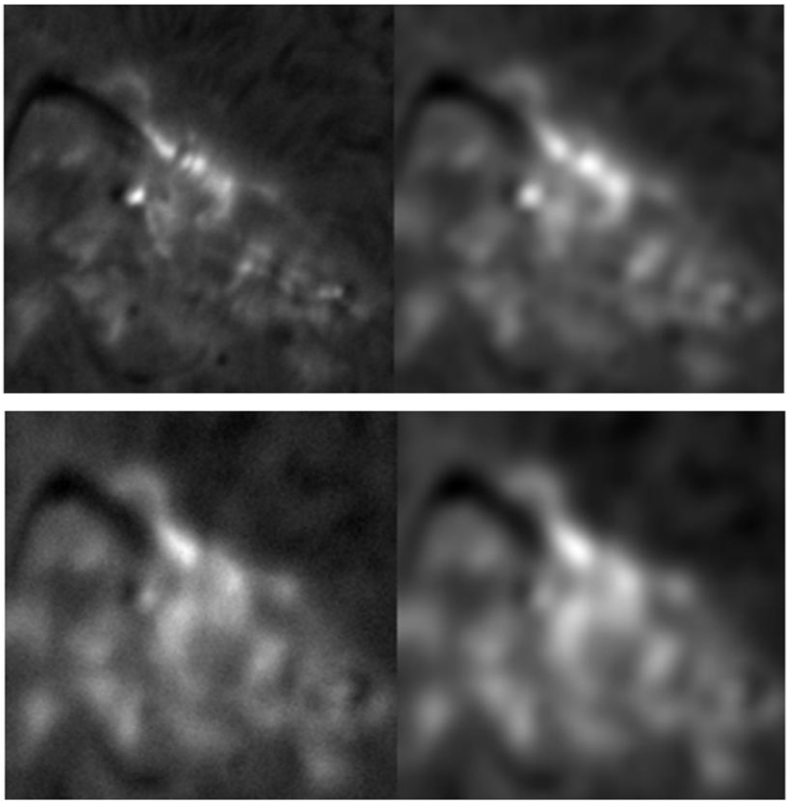

Figure 16. Image Sharpness Examples. The smoothed images are on the right and the original images on the left. The two top row images, with a sharpness value of 0.0228 are from the example used during this chapter, Cerro Tololo, Chile, at 14:28:34 UT on 3 August 2011. The two on the bottom are from the GONG site at El Tiede, Canary Islands, with an image time of 14:45:14 UT on the same day and a sharpness value of 0.0086.

applying the smoothing function yields a large difference between the original image and the smoothed image (right). The bottom case is an example of where the original image (left) is already somewhat blurred by site seeing conditions, so applying the same smoothing function yields less of a difference between the smoothed image (right) and the original. Sharpness magnitudes in this project ranged from about 0.006 to 0.040. Figure 17 shows an example of the time variation of the sharpness parameter during at 1F

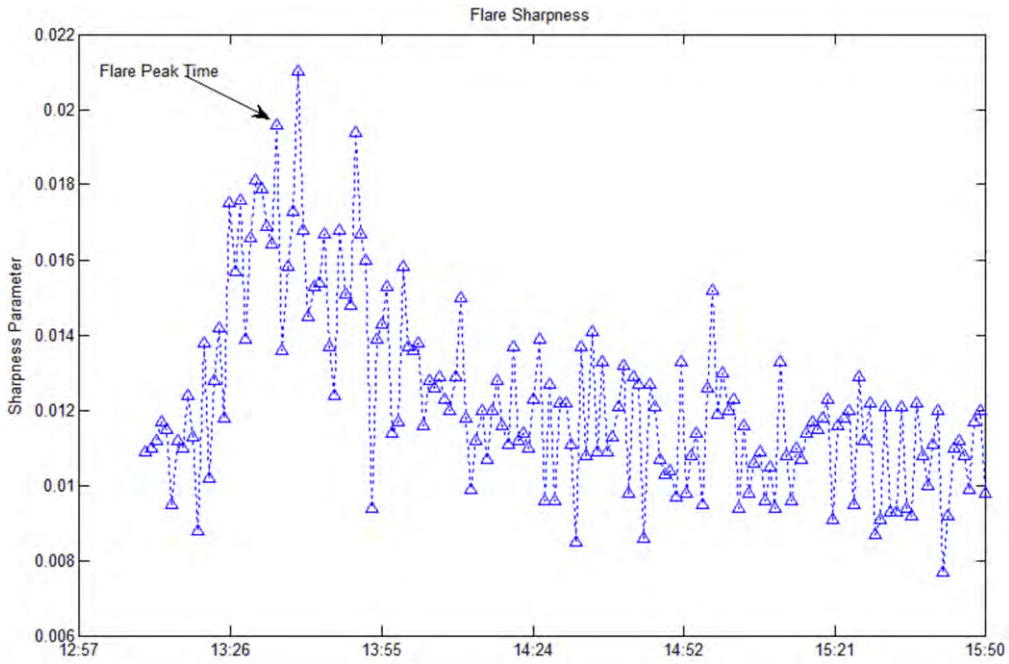

Figure 17. Flare Sharpness Time Evolution from the GONG site at El Tiede, Canary Islands. A 1F flare was observed during this period on Aug. 3, 2011 and the flare peak time was 13:34 UT.

flare observed at El Tiede on Aug. 3, 2011. Noteworthy is how the atmospheric seeing conditions are in a constant state of flux as is denoted by the variability of the sharpness from minute to minute along the vertical axis. The flare peak time is noted on the plot, and is one of the highest sharpness values during the flare. The sharpness parameter is found to play a significant factor in flare rating determination (Chapter 4).

3.3.5 Steps Involved in Running the Code

There are a few steps involved in running the IDL code used to analyze solar flares for this project. The first step is selecting a flare for analyses. As mentioned before, this is determined based upon the SOON text bulletins. The bulletins provide the flare start and end times, and GONG imagery for these times (plus 10 minutes on either side—see Section 3.2.2) is downloaded from the GONG website. The SOON text bulletins also contain the solar region number where the flare was located (Item 'O' in Figure 12) as well as the coordinates relative to the center of the disk (Items 'G' and 'H' in Figure 12). The next step is to open a GONG image near the SOON flare peak time with a FITS viewer program (many are freeware obtained online). By using the FITS viewer program one is able to obtain the pixel coordinates of the flaring region which is where the regional box (Section 3.2.2) is centered. These coordinates, as well as the dimensions of the box, are entered directly into the source code of the IDL program. Also specified in the source code at this time is the directory path to the imagery on the local computer, as well as which observatory's imagery is to be analyzed. This is done by using the two-letter observatory identifier: Bh for Big Bear, Mh for Mauna Loa, Lh for Learmonth, Uh for Udaipur, Th for El Tiede, and finally Ch for Cerro Tololo. Finally the code is ready to be run, scanning and processing every image for the specified observatory in time order, calculating each time flare intensity, corrected area, and sharpness. Once the code has finished processing all the event data, a plot is created and displayed of brightness, area, or sharpness (see Figures 5 and 17). The code also outputs an ascii-formatted text file containing all of the parameters calculated for all iterations.

4. Analysis and Results

4.1 Chapter Overview

This chapter summarizes the results of the analysis of solar flares in both SOON and GONG systems. First is a SOON to SOON comparison that contains all flares in which two SOON sites witnessed the same flare. Next is an intra-GONG comparison of flares that were seen by at least two GONG sites. Following this comparison, these and other larger GONG flares as compared to SOON flares. Finally GOES X-ray flares are used to find GONG imagery of flares not seen by SOON observations due to various reasons.

4.2 SOON to SOON Comparison

The first evaluation was to compare observations from within the SOON network. This was done to gauge the degree of consistency between two SOON sites that observe the same flare. The period of examination was from March 11 through November 30, 2011.

4.2.1 Initial Results of Analysis

As mentioned in Chapter 3, the SOON flare text bulletins were used to perform comparisons within the observing network (and later to GONG imagery), due to the non-calibrated SOON archived imagery. During this period, there were a total of 124 flares that were seen by two SOON sites. Of these, there were 114, or 92% of the total, that received the same brightness and area ratings by both sites. The brightness and area breakdown of these 114 events are listed in Table 5. As can be seen, the vast majority of

these flares are of the subflare (0F) variety, which is consistent with results found by Temmer, et al (2001).

Table 5. Flares Observed by Two SOON Sites

		Brightness				
		Faint	**Normal**	**Brilliant**	**Total**	**Percent**
Importance	**0**	107	1	0	108	94.7
	1	0	2	0	2	1.8
	2	0	1	3	4	3.5
Total		107	4	3		
Percent		93.9	3.5	2.6		

Of the ten flares that did not receive the same brightness and area ratings, there were three flares in which the only difference was a one category brightness rating, four flares in which the only difference was a one category area rating, and three flares in which there was a one category difference in each brightness and area (Table 6). There were no cases in which there was a two category difference.

Of all the flares that received the same area category rating, the average corrected area was 48.5 millionths, while the average difference between the two sites witnessing the same flare was 16.2 millionths. For the seven remaining flares where the area rating differed between the two sites (see Table 6) the average corrected area was 98.4 millionths, while the average difference in flare corrected area between sites was 49.4 millionths.

Table 6. SOON Intersite Discrepancies

Number of Occurrences	Lesser Flare	Greater Flare
3	0F	1F
1	0F	0N
4	0F	1N
2	1F	1N

Recall from Section 3.2.1, in the SOON system the 10th bin has a brightness level of the quiet sun, the 16th bin is typically considered a faint flare (1.6 times the background), the 27th bin a normal flare, and the 36th bin a brilliant flare. Of all the flares that received the same brightness rating, the average brightness difference between the two sites witnessing the same flare was 1.8 brightness bins. For the seven remaining flares where the brightness rating was differing between the two sites, the average difference in brightness was 4.8 brightness bins.

4.2.2 Solar Elevation Angle Consideration

In examining the cases in which flares did not receive the same brightness and/or area rating, the sites' solar elevation angles were estimated. The solar elevation angle is defined as the angular distance measured from the horizon to the sun, along a line defined by the sun and local zenith. The maximum solar elevation angle possible is 90 degrees when the sun is located at the zenith (only occurring in equatorial regions) and the minimum of zero degrees occurs at sunrise and sunset. When the solar elevation angle is low, solar radiation takes a longer path through the earth's atmosphere, leading to increased scattering. Additionally, the beam path is also longer nearer to the ground

where turbulence and mixing cause variations in atmospheric seeing. The effects of the atmosphere did seem to be affecting the flare measurements, since in eight of the ten cases, the lesser area and/or lower brightness rating occurred at the site that had the smaller solar elevation angle. For these eight cases, the average 'higher' solar elevation angle was 34.7 degrees and the average 'lower' solar elevation angle was 9.1 degrees. There was one case where the opposite of what one might expect occurred—the site with the higher elevation angle actually had the lower area/brightness rating. Also surprisingly, in this case, the site with the lower solar elevation angle also had clouds during portions of the flare event yet still measured a higher area/brightness. No explanation is available for this discrepancy. Finally, one of the 10 flares was a case where both sites had the same solar elevation angle (33 degrees), yet there was a one category disparity in area and brightness. In this case there were no clouds noted by the observer at either observatory. For this case also, there is no explanation available for the discrepancy between sites.

Figure 18 and Figure 19 show the comparison of area and brightness ratings for all the flares that two SOON sites observed. In these plots, the SOON site that had the low solar elevation angle between the two was plotted on the horizontal axis and the site with the higher solar elevation angle was plotted on the vertical axis. The blue data points indicate where area or brightness categories were the same between sites and the Both figures show that there are some instances where area or brightness categories may differ, but actual values are rather similar. For example, in Figure 19, there is a flare where the site with the low solar elevation angle observed a flare intensity of 2.8 times

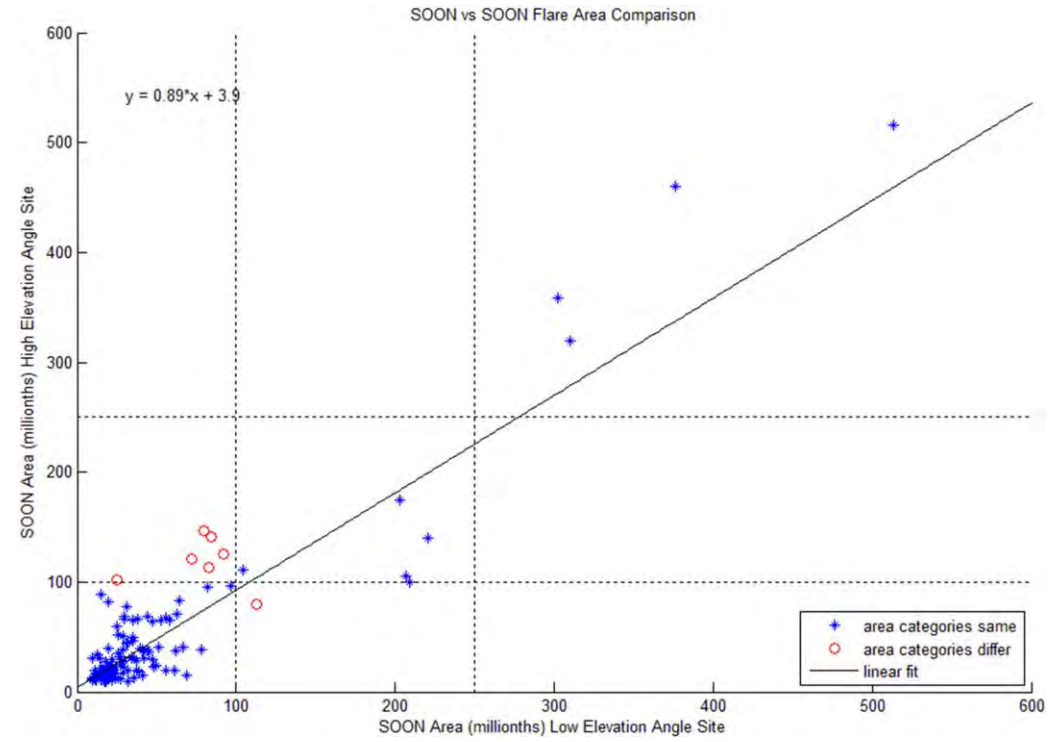

Figure 18. SOON vs SOON Flare Area Comparison

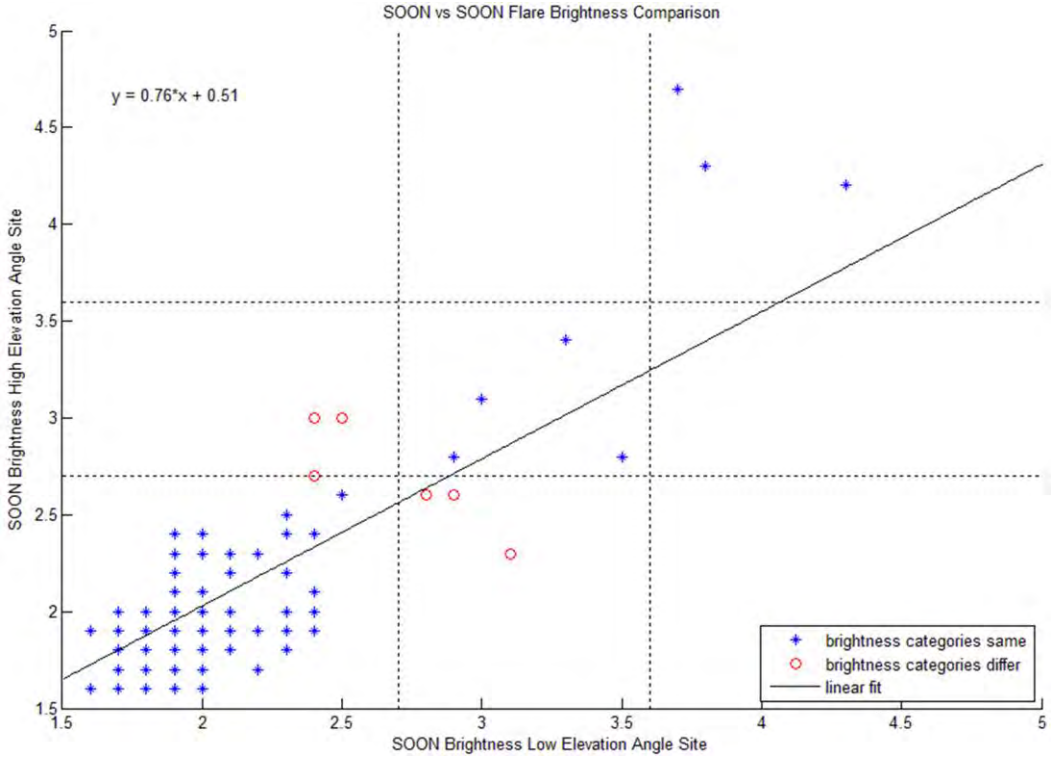

Figure 19. SOON vs SOON Flare Brightness Comparison

the background where the site with the high solar elevation angle observed the same flare having an intensity of 2.6 times the background. There are other instances where there is a greater difference in intensity between sites yet the ratings still fall within the same brightness category. Similar instances applied to flare area are noted in Figure 18.

4.2.3 Observation Quality Factor

In addition to checking the solar elevation angle, the observation quality rating from the SOON sites was considered as a possible factor in category differences between sites. Recall from Chapter 3 that the SOON sites report observation quality on a scale from 1 to 5, with a rating of 3, 'fair' quality, being the default. In the ten flares where there was a difference between SOON brightness or area categories, the quality of the observation was rated as 'fair' from both sites in nine cases. There were three cases where clouds were present at some portion of the observation yet the 'fair' rating was still assigned. These were also three of the eight that had a lower solar elevation angle and measured a lesser area/brightness. There was only one flare in which one site rated the quality 'poor' and observed 'normal' flare brightness, and the other 'very poor' observation quality with a 'faint' flare brightness. In this case, the site which rated the quality 'very poor' also had the smaller solar elevation angle and clouds were noted by the observer.

4.2.4 Differences in Flare Peak Times

Sometimes there are differences in peak flare times when two SOON sites observe the same flare. Since flares are rapid events, it was necessary to check to see if the observation time difference between the observatories was a reason why some of the observatories reported different categories for the same event. For example, if one site

observed a 1N flare with peak intensity at a certain time and the other site observed a 2F flare with peak intensity four minutes later, perhaps a factor in the difference between the reported flare categories was due to a difference in the times of peak flare intensity. Table 7 gives the results of the time difference comparison. In this case there were many more flare category matches than not, and the average difference in observation time was less than two minutes. However when there is a difference in brightness or area category between sites the average flare peak time difference does increase slightly.

Table 7. SOON Time Difference Between Sites

Characteristic Between Sites	Number of Occurrences	Average Time Difference (minutes)	1-Sigma Error
Area Categories Match	117	1.7	1.9
Area Categories Differ	7	2.0	1.8
Brightness Categories Match	117	1.6	2.1
Brightness Categories Differ	7	3.6	4.0

4.2.5 SOON to SOON Conclusion

In conclusion, the overall variability within the SOON network was 8%, since 10 of 124 total flares observed by two SOON sites received different category ratings. When considering flares in which at least one site observed a flare greater than subflare, the variability increased to 55%, or 10 of 18 flares. For event-level flares (greater than 2B) there was no variability (0%) since in all three flares, both SOON sites observed rated the flare 2B.

4.3 GONG to GONG Comparison

Next was a comparison of flares as seen by the GONG system to gauge the amount of consistency from site to site before taking the next step of making a comparison of GONG to SOON.

4.3.1 Comparison Using Flares Observed by Two SOON Sites

The first dataset of flares for comparison were the same 124 flares from Section 4.2 in which two SOON sites observed the same flare. As it turned out most of these flares could not be included in a GONG to GONG comparison for a number of reasons, outlined below in Table 8.

Table 8. GONG Flares Where Two SOON Sites Observed

Number of Occurrences	Characteristic
48	Only one GONG site observing
9	At least two sites observed, but minimum flare criteria not met
3	Limb flare where IDL algorithm could not be run accurately
21	Unavailable or incomplete imagery
12	At least two sites observed, but only one gave a minimum flare rating
31	At least two sites observed and provided a rating

There were 43 total flares that at least two GONG sites observed. If three or four GONG sites observed a flare, then the two sites with the largest/brightness ratings were used for comparison. In one flare the difference in flare peak brightness times between GONG sites was 20 minutes so this flare was discarded from the comparisons. Of the 42

remaining flares, 26 of the cases (62%) were observed with the same brightness and area rating. In 12 of the 42 (29%), only one site observed the event as a flare. The observation at the other sites did not reach flare status due to not meeting the minimum area threshold of 10 millionths. In these twelve cases, the site with the higher sharpness is the site that met minimal flare criteria in nine cases or 75% of the time. In two of the twelve cases the site with the lower sharpness is the site that met minimum flare criteria (17% of the time). In the last case, sharpness data was not calculated because running the algorithm required drawing a local box around the near-limb flare that was too small (less than 180 by 180 pixels). Recall from Section 3.3.3 that the sharpness algorithm requires a minimum image size of 180 by 180 pixels. For the remaining 4 of 42 cases (10%), both GONG sites observed minimum flaring thresholds and there was a category difference in either area or brightness. There were three of these in which the site which rated the flare as less bright or smaller had the lower sharpness between the two sites. The remaining case was a flare near the solar limb in which the sharpness algorithm could not be run because, once again, the box selected around the flare was limited in size to avoid sampling the region beyond the limb.

There were various reasons why the other cases in Table 8 could not be utilized in the GONG to GONG comparison. For the first 48 cases, there was only one GONG site providing observations; in these cases a second GONG site was not available for comparison. There were nine cases in which two GONG sites observed the same flare but minimum flare criteria (brightness or area) was not met. Recall that the majority of the SOON flares were 0F and many of these barely met minimum flare thresholds. Thus in some of these cases GONG ratings were similar but slightly smaller/fainter and did not

meet minimum flare criteria. There were three flares where running the IDL algorithm was problematic because the flare could not be sampled without also sampling the region beyond the solar limb. There were 21 cases in which GONG imagery was unavailable or incomplete online. Twelve of these 21 cases occurred over just three days—28 and 29 July and 16 October. For the July case, it did seem that weather might have played a role in the missing data, as radiometer data from three GONG sites indicated clouds affecting observations. For the October case, radiometer data did not indicate clouds; however system status information is not available so it is difficult to conclude why GONG data was not present. The remaining nine cases with missing GONG data were scattered across different dates and were likely weather or maintenance related.

4.3.2 Comparison Using SOON Flares Greater Than 0F

In order to increase the number of flares for comparison between GONG sites from the 42 considered above, another set of flares was examined. This next comparison includes all the GONG imagery available for flares larger/brighter than a SOON rating of 0F, observed from March 11 to November 30, 2011. There were a total of 100 of these flares and in 47 instances two or more GONG sites had imagery available and a flare rating could be determined by running the IDL algorithm. Two of the 47 were cases where two SOON sites had also observed, and were already considered in the previous section. One flare had a difference in peak times between GONG sites of 17 minutes and this flare was also discarded from the comparison.

For these additional 44 flares that at least two GONG sites observed, both of the sites rated the flare with the same brightness and area categories in 22 instances. Once again, if three or more GONG sites observed a flare, then the two sites with the

largest/brightness ratings were used for comparison. Of the 22 remaining cases, analysis of GONG imagery yielded at least one site giving the flare a different area or brightness category rating than the other(s). In 19 of these cases there was sharpness data available. And 95% of the time (18 of the 19 cases), the site with the lower brightness or smaller area rating was also the site with the smaller sharpness rating as determined by the sharpness algorithm. There was only one case in which the opposite was true (the smaller sharpness value yielded the larger flare area). In looking at this case more closely, there was no indication that clouds played a factor. The difference in sharpness was 0.003, which is a relatively small difference between sites. For the remaining four cases, the sharpness data was unavailable because the box selected around the flare was limited in size to avoid sampling the region beyond the limb.

Figure 20 is a visual depiction of how sharpness affects flare rating within GONG. The image on the left, from the observatory at Big Bear, has a sharpness value of 0.0281, and the image on the right, from Cerro Tololo, has a sharpness value of 0.0139. The difference in sharpness accounted for a difference in area category, as Big

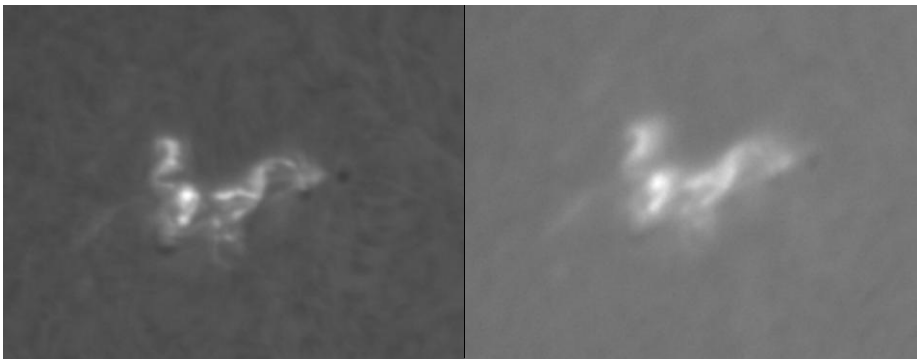

Figure 20. GONG Sharpness Difference Example. The image on the left is a 1F flare with a sharpness value of 0.0281 while the image on the right is a 0F flare with a sharpness value of 0.0139. Both images are from 27 Jul 2011, 16:05 UT.

Bear rated the flare a 1F while Cerro Tololo rated the flare a 0F. These findings support the usefulness of the sharpness algorithm to resolve event classification discrepancies between sites.

4.3.3 Solar Elevation Angle and Sharpness Comparison

Recall for the SOON to SOON comparison case, while sharpness data was not available, there was at least some indication of solar elevation angle being a possible reason for intersite differences. In the GONG case, with the algorithm already computing sharpness, solar elevation angle was calculated to see if any correlation can be made between sharpness and solar elevation angle (Peat, 2011). Figure 21 shows GONG sharpness parameter compared to solar elevation angle for all the flares rated above 0F by SOON sites, during the time period of this review. Every GONG flare rating that had a sharpness parameter available was plotted with the corresponding solar elevation angle.

As is represented in the plot, the data was sorted according to sharpness parameter, from smallest to largest. The plot indicates that there little if any correlation between sharpness and solar elevation angle. One notable difference in this dataset compared to the SOON set where solar elevation angle was a determining factor is the much wider variety of solar elevation angles in the GONG case plotted above. Because SOON sites are more widely spaced than GONG sites, one SOON site will always have a low solar elevation angle compared to the other if they are viewing the same flare. Recall that the average 'low' solar elevation angle in the SOON to SOON comparison was only 9 degrees. In the GONG case, the solar elevation angles vary from 0.5 to 85 degrees. This may be a reason why solar elevation angle may be more of a factor in the SOON to SOON comparison because of the necessarily low solar elevation angles involved.

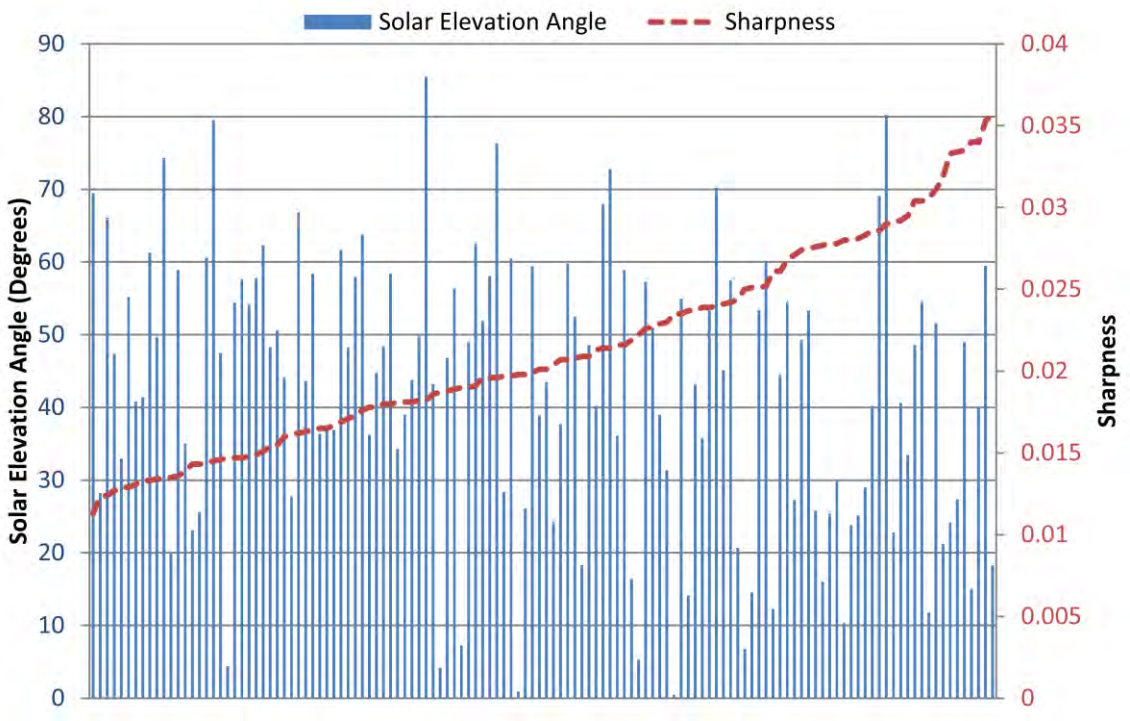

Figure 21. GONG Sharpness Parameter and Solar Elevation Angle.

When sharpness data at the time of flare peak brightness was sorted according to each GONG site, the results are given in Table 9. For this set of flares it turns out that the GONG site at Big Bear has a higher average sharpness than the other five sites. It is not surprising that Big Bear ended up having the highest sharpness parameter in this small data sampling, as it is well known for its favorable atmospheric seeing conditions, as noted by Hill (1994) and Verdoni (2007). The small sample size prevents firm conclusions from being drawn, especially regarding the other sites. Also, the sharpness parameters used in this review are simply a snapshot in time, taken at the time of maximum flare brightness. Recall Figure 17 in Chapter 3 that shows the variability of the sharpness parameter through the duration of a flare.

Table 9. GONG Site Sharpness Comparison

Site	Average Sharpness / (1-sigma error)	No. of Measurements Based Upon
Big Bear	0.024 +/- 0.006	24
Cerro Tololo	0.022 +/- 0.007	25
Learmonth	0.021 +/- 0.005	18
Mauna Loa	0.020 +/- 0.006	18
El Tiede	0.019 +/- 0.005	30
Udaipur	0.020 +/- 0.006	13

Figure 22 and Figure 23 show the comparison of area and brightness ratings for all the flares that two GONG sites observed. In these plots, the GONG site that had the higher sharpness between the two was plotted on the horizontal axis and the site with the lower sharpness was plotted on the vertical axis. Once again, data points are color coded according to whether area or brightness categories matched (blue) or differed (red). There are also instances on these plots that show where area or brightness values may be similar, yet fall in different categories or be disparate yet still fall in the same category.

4.3.4 Differences in Flare Peak Times

Similar to the peak time comparison in the SOON network, the same analysis was performed to flares that were observed by two GONG sites. Table 10 gives the results of the time difference comparison. Here the total number of flares was 74. This comes from the 30 flares from Section 4.3.1 plus an additional 44 from Section 4.3.2. The average difference in flare peak time was less than two minutes, even slightly less than in

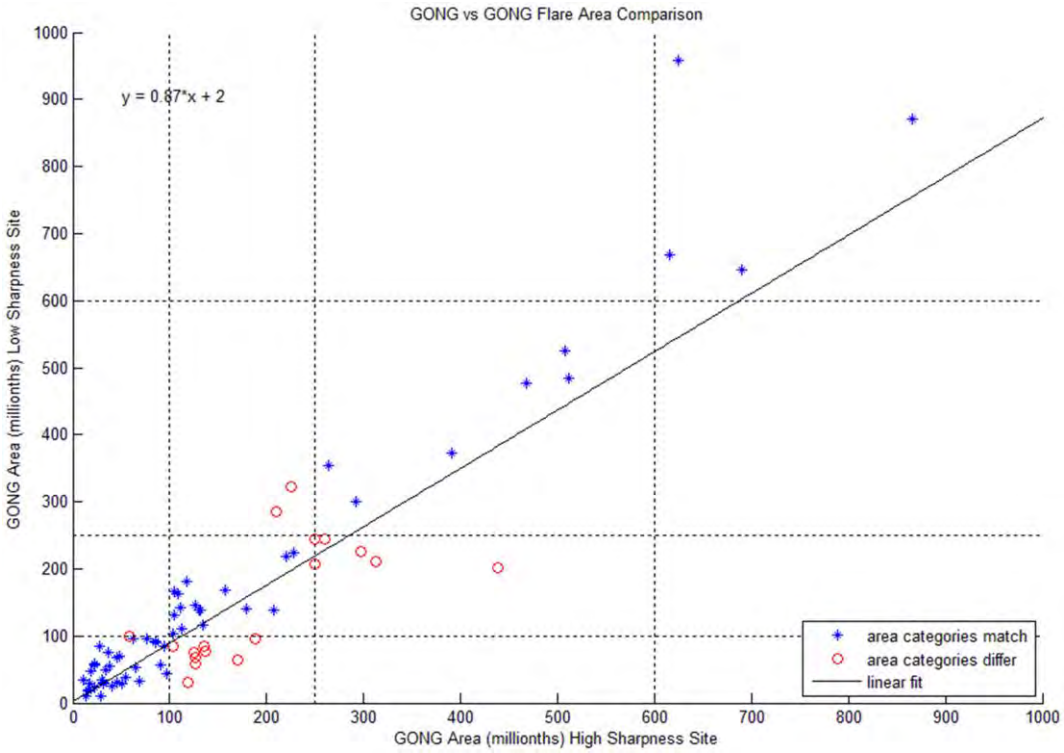

Figure 22. GONG vs GONG Flare Area Comparison

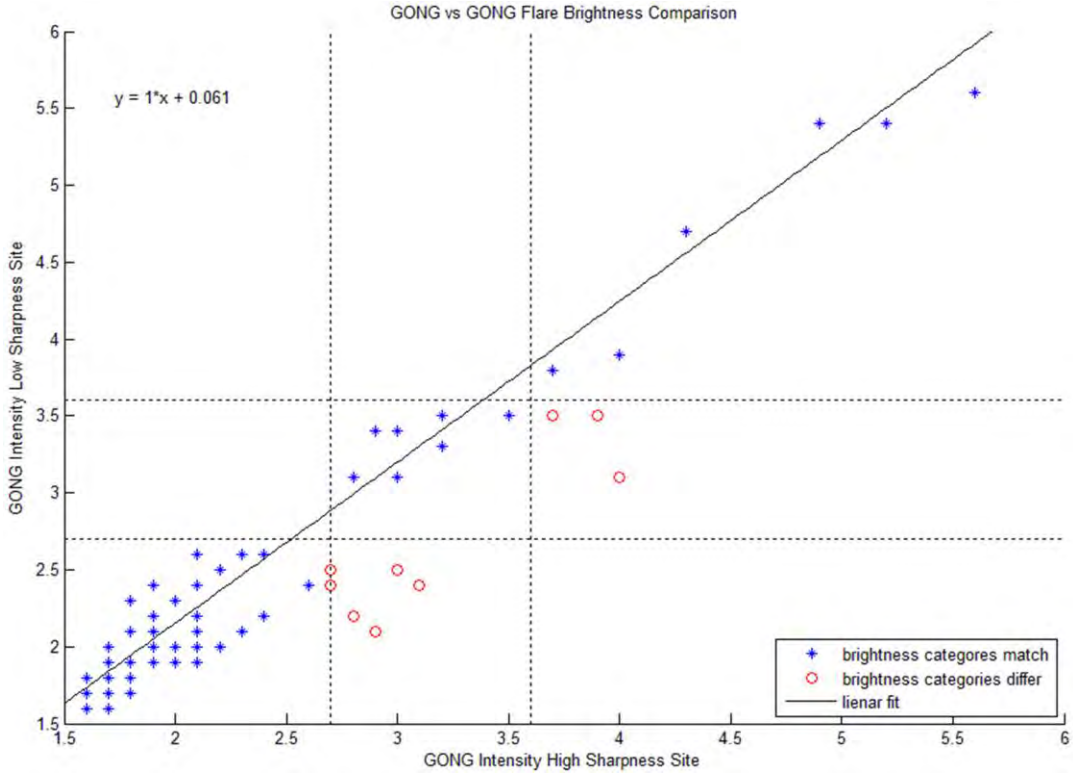

Figure 23. GONG vs GONG Flare Brightness Comparison

the SOON to SOON comparison. Here there was no indication of an increased peak time difference being related to a difference in area or brightness categories.

Table 10. GONG Time Difference Between Sites

Characteristic Between Sites	Number of Occurrences	Average Time Difference (minutes)	1-Sigma Error
Area Categories Match	56	1.4	1.5
Area Categories Differ	18	1.4	1.4
Brightness Categories Match	65	1.4	1.5
Brightness Categories Differ	9	1.0	0.8

4.3.5 GONG to GONG Conclusion

In conclusion, while it is not always the case that a given flare will rate as the same area and brightness among two or more sites in the GONG network, there are very few instances where a difference in sharpness does not offer a reasonable explanation for the difference. A strong correlation between solar elevation angle and sharpness was not found. Thus the sharpness parameter is the better factor to resolve brightness and area discrepancies among GONG sites.

The overall variability within the GONG network was 44%, since 38 of the 86 total flares observed by two GONG sites received different category ratings. When considering flares in which at least one site observed a flare greater than a subflare, the variability increased to 60%, or 26 of 43 flares. For event-level flares (greater than 2B) the variability decreased to 38%, or 3 of 8 flares, where in five cases both GONG sites rated event-level flares as having the same category.

It is also worth noting that when compared to SOON, where the overall variability rate was only 8% (Section 4.2), there was more variability in GONG category rating, where 44% of flares seen by multiple sites received a different rating between sites. One possible reason for this is that most SOON flares were subflares. When comparing flares greater than subflares, the variability between the two networks is similar—55% in SOON to 60% in GONG.

4.4 SOON to GONG comparison

For the SOON to GONG comparison, all SOON flares larger than 0F from March 11 to November 30, 2011, were considered. The distribution of these 100 flares follows below in Table 11, identical to Table 4 except in the omission of 0F flares. Of these 100

Table 11. SOON Flares Greater than 0F

Importance \ Brightness	**Faint**	**Normal**	**Brilliant**
0		12	0
1	44	24	4
2	1	6	8
3	0	0	1
4	0	0	0

flares, eleven of them were seen by two SOON sites and were included in the SOON to SOON comparison of Section 4.2. For the purposes of the comparison in this section, the

larger and/or brighter of each of the eleven pairs of SOON observations were used, thus avoiding double counting.

Of the hundred flares greater than 0F, there were 89 GONG counterparts that were able to be rated when running the IDL code, and there was one additional case where the GONG flare did not meet minimum flare brightness criteria. This was observed by SOON as a 1F flare and no rating was assigned for GONG. This flare will be included in the overall variability calculation between the two networks, but will not be included in the brightness and area comparisons because no GONG flare rating was determined. The remaining ten cases either had no GONG imagery available, or were limb events where creating a box around the flaring region necessitated including regions beyond the solar limb, or were discarded due to inconsistencies with the SOON text bulletins (Table 12). None of the eleven flares not rated by GONG were 2B or greater in

Table 12. GONG Flares Where SOON Observed Greater than 0F

Number of Occurrences	Characteristic
2	Limb flare where IDL algorithm could not be run accurately
5	Unavailable or incomplete imagery
3	Discarded because of inconsistencies with SOON text bulletins
1	At least one site observed, but minimum flare criteria not met
89	At least one site observed and flare rating was available

SOON. For the three cases that were discarded due to inconsistencies, when running the GONG algorithm, no brightening of the solar active region was detected during the

period beginning 10 minutes before the flare start time to 10 minutes following the flare end time in the SOON text bulletin. There is no explanation for this except that there may have been an error in the SOON text bulletin. For one of the three cases this was obvious, because the flare start and end times were the same but the peak time was 37 minutes later. For this case, no brightening was observed in the imagery or detected by the algorithm before, during or after the peak flare time noted in the text bulletin.

For some of the flares, there were multiple GONG sites that observed the flare, and the code was run on all of the imagery available. In the cases where one, two, or three (rarely four) GONG sites observed, a determining factor was needed to decide which GONG site's flare rating would be used to compare against SOON. If multiple GONG sites observed the same flare, then the site with the largest or brightest flare was chosen as the having the 'best' flare rating and was used in the SOON comparison. In most cases this was the flare with the highest sharpness. There were five flares of the 89 in which the difference in flare peak times from SOON to GONG was greater than 10 minutes. These five flares were discounted for the remaining comparisons, leaving 84 left over. Table 13 shows a comparison between what the SOON observatories reported and how this compared in the IDL analysis of the imagery from GONG. The red squares represent the cases where both SOON and GONG both rated the flares as having the same brightness and area categories. For example, there were 31 SOON flares rated 1F and of these, 17 (or 55%) were also rated by GONG as 1F. However, of these 31, GONG rated 9 (or 29%) as 0F, two (or 6%) as 1N, and three (or 10%) as 2F. All of the cases in the lower-left portions of the table depict where the SOON rating was either brighter and/or larger in area than the GONG rating, and all of the cases in the upper-right

Table 13. SOON vs GONG Flare Comparison

SOON Rating \ Best GONG Rating	0F	0N	0B	1F	1N	1B	2F	2N	2B	3B
0F										
0N	7			4	1					
0B										
1F	9			17	2		3			
1N	5			7	3			4	2	1
1B						1		2	1	
2F							1			
2N				2			1	2		
2B					1			1	4	2
3B										1

portions show where the GONG rating was either was either brighter and/or larger than the SOON rating.

Of the 84 cases, there was only one case in which there was more than a one category difference of either area or brightness rating between SOON and GONG. This was the case on the far right of Table 13 where the SOON observatory rated the flare a 1N while the GONG rating was 3B, which meets event-level criteria. There were clouds noted in the SOON observation, offering a plausible explanation for the significant rating difference.

4.4.1 Comparison Based on Area Only

Another way of examining how the flares were rated in the two observing networks is by comparing flare area (Table 14). Of the total 84 flares, there were 47

Table 14. GONG Relative to SOON Importance Comparison

	GONG Category	Match with SOON	SOON One Category Higher	SOON One Category Lower
Area	**0**	7	14	
	1	30	3	5
	2	9	0	12
	3	1	0	2
	Total	47	17	19
	Percent	56.6	20.5	22.9

instances where the area category matched between SOON and GONG. There were 17 instances where the SOON rating was a category higher than the GONG rating and 19 instances where the GONG rating was a category higher than the SOON rating. This suggests that on average the area ratings between the two systems are relatively well balanced, and are not biased towards one system giving a predictably different rating than the other system.

Another way of examining area differences is to compare actual area values directly, instead of merely area categories. The results of such a comparison are depicted in the scatter plot in Figure 24. The points in the plot are color coded according to

whether there was agreement between area categories or not. A least-square linear fit was assigned the data, represented by the solid black line. The flare affected by weather (mentioned above) where SOON observed at 1N and GONG a 3B was plotted, but not included in the linear fit. The plot shows that the linear fit has a slope of greater than one; this indicates that there is a tendency for GONG flare area to be slightly higher than

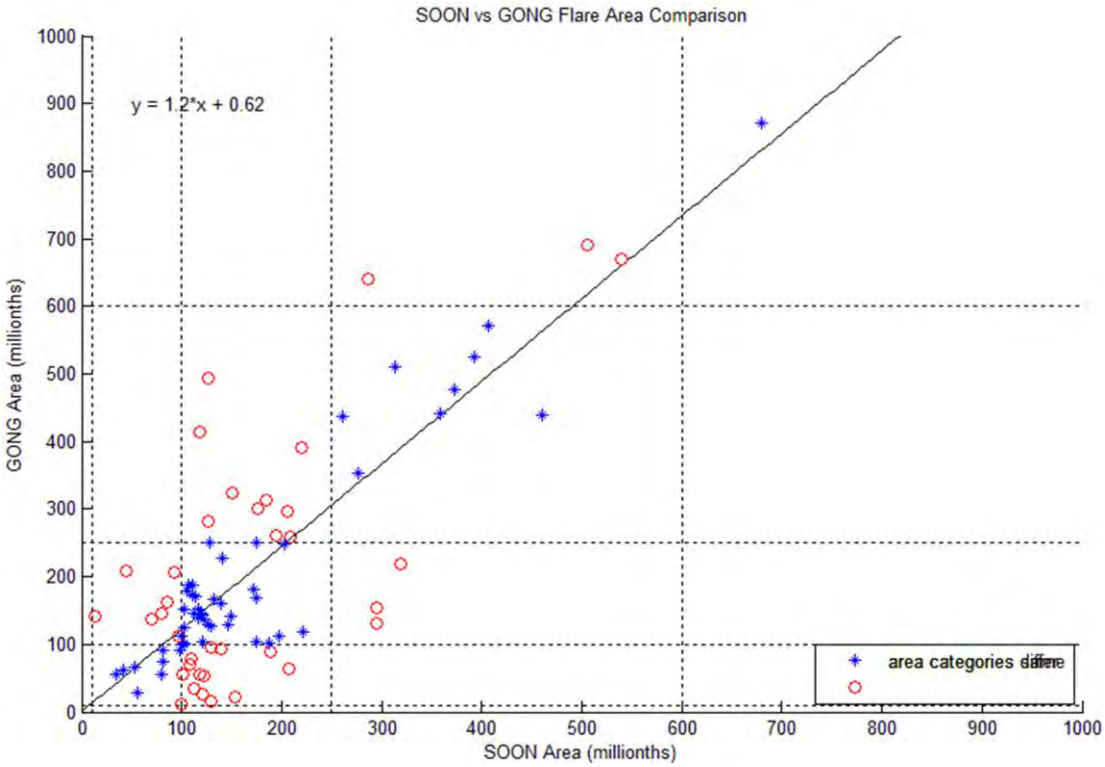

Figure 24. SOON vs GONG Flare Area Comparison

SOON flare area. For this plot, the error estimation of the linear fit coefficients, in addition to the coefficient of determination (R^2), was calculated to evaluate how well the estimated linear regression line fits the data. A value of R^2 close to one indicates a good fit—that the independent variable explains most of the variability in the dependent variable. A value of R^2 close to zero indicates that the fit is not much better than the

model $y = constant$ and the linear regression model is of little use (Rosenkrantz, 2009). In this case, the standard errors (or deviations) of the linear fit coefficients are 18.9 for the intercept and 0.09 for the slope of the linear fit. Additionally, $R^2 = 0.477$, which indicates a fair linear fit. This value may seem a bit low, but there is a notable amount of variability between areas measured by the two instruments. One possible reason for this is that the area calculation algorithms between the two are different (the IDL algorithm on the GONG data and the videometer at the SOON sites). As an example of the variability, for all SOON area measurements between 100 and 250 millionths (area category '1'), GONG area measurements range from about 10 to 500 millionths, despite still falling within only one category difference.

It is also worth noting that flare area values may be quite similar between networks, but may still fall in different area categories. This is seen by the flare represented by a red point where the SOON area is just under 100 millionths but the GONG area is just over 100 millionths. Conversely there are some flares in which there is a difference in area categories that actually have a lesser difference in actual area values than some flares of the same category between the two networks.

4.4.2 Comparison Based on Brightness Only

When comparing brightness categories, there was some noticeable difference between the two systems, and this is seen in Table 15. While the number of cases where brightness categories were the same between systems was similar as for area categories (49 cases), in cases where there was a difference in brightness rating, the SOON system had the brighter flare rating in 30 cases. On the other hand, the GONG system had the brighter flare rating in only 5 cases. This difference was most notable in the faint to

Table 15. GONG Relative to SOON Brightness Comparison

Brightness	GONG Category	Match with SOON	SOON One Category Higher	SOON One Category Lower
	Faint	30	26	
	Normal	10	4	2
	Brilliant	9		3
	Total	49	30	5
	Percent	58.3	35.7	6.0

normal flares. Of the 58 total flares where at least one network rated the flare as having faint brightness, there were 26 flares where SOON rated the flare as having normal brightness, 30 instances where both networks rated flares as faint, leaving only two instances in which GONG rated normal and SOON rated faint. In the cases where at least one network rated a flare as brilliant, the agreement between them was improved, and 56% of flares were rated the same brightness between both systems. Finally, a point worth noting is that in Table 15 there are a total of 84 flares while in Table 14 a total of 83. This is due to the single flare not included in which there was a two category (1N to 3B) importance difference between SOON and GONG, as noted in Table 13.

Brightness differences were also compared using actual brightness values, instead of considering just category differences. The results of such a comparison are depicted in the scatter plot in Figure 25. Similar to Figure 24, the points in the plot are color coded according to whether there was agreement between brightness categories, and a linear fit was assigned the data. In this case, the linear fit has a slope near one, however it is

shifted to the right of where the $y = x$ line would fall. This confirms the data shown in Table 15, that SOON flares have a tendency to be brighter than GONG flares. Also in this case, flare brightness values may be quite similar between networks, but may still fall in different brightness categories. The standard errors of the linear fit coefficients are

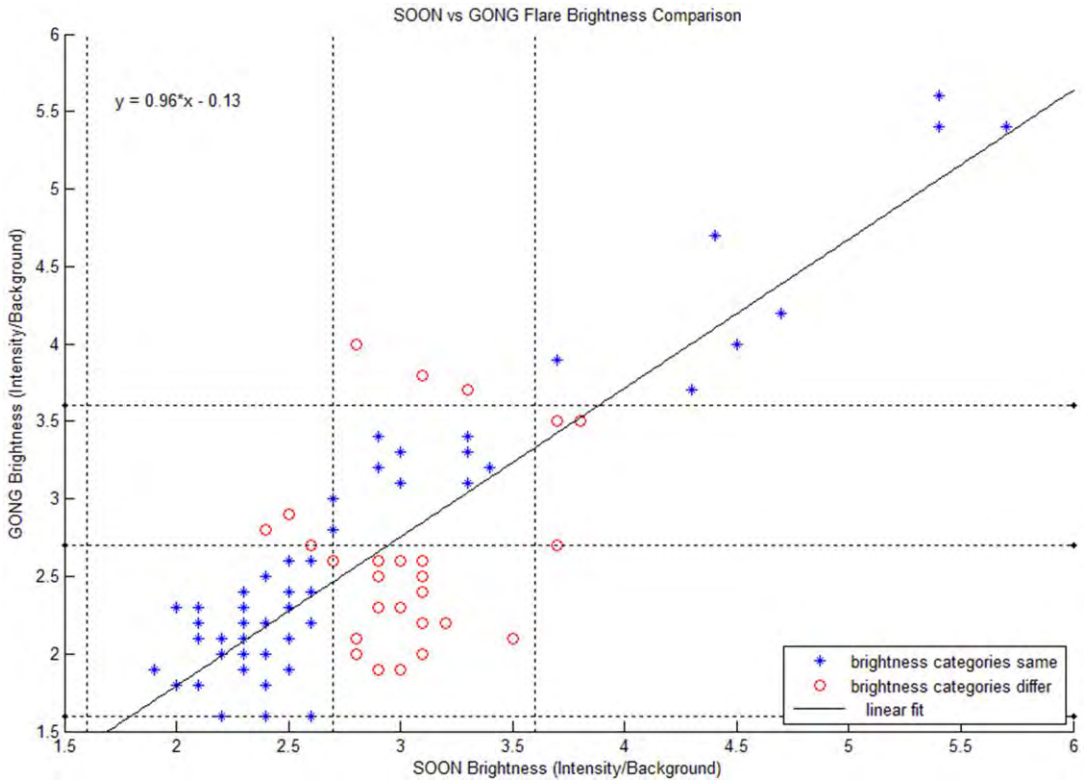

Figure 25. SOON vs GONG Flare Brightness Comparison

0.18 for the intercept and 0.06 for the slope. The coefficient of determination, R^2, was calculated to be equal to 0.738. This indicates a linear fit with less error than was seen in the area comparison.

4.4.3 Event-Level Flare Comparison

Recall that event-level flares are those defined as those rated 2B or larger/brighter. During the period of study, there were nine event-level flares as reported by the SOON observatories. Eight of these were rated 2B and one was rated as 3B. Following in Table 16 are further details for these particular flares. For these event-level

Table 16. SOON Event-level Flares and GONG Ratings

2011 Date / UT	SOON Rating / GONG Rating	GONG Sharpness / SOON Quality	Comments
3 Aug / 1350	2B / 1N	0.0228 / 3	
4 Aug / 0355	2B / 2B	0.0271 / 3	
9 Aug / 0806	2B / 2B	0.0216 / 3	
6 Sep / 2221	2B / 3B	0.0304 / 3	Flare in progress at sunset at SOON site
7 Sep / 2238	3B / 3B	0.0311 / 3	Flare observation ended prematurely at SOON site due to clouds
24 Sep / 0936	2B / 2B	0.0319 / 3	Flare in progress at sunset at SOON site
25 Sep / 1531	2B / 3B	0.0280 / 3	
26 Sep / 1443	2B / 2N	0.0286 / 3	
3 Nov / 2023	2B / 2B	unavailable / 3	

flares, 56% of the time GONG rated in the same category of brightness and area as SOON, 22% of the time GONG rated lower by one category of brightness or area, and 22% of the time GONG rated higher by one category of brightness or area. In all nine cases, the SOON observation quality was rated the default 3, or 'fair' quality. For the

cases where there was a difference in category, it was not always obvious to determine a certain reason for the differences. In the case from 3 August, GONG observed the flare peaking 16 minutes before SOON followed by a gradual decline, though it is unknown what the SOON flare evolution was during this time because only the flare peak time is known. The disparity in peak time is a good reason why there was a difference, since flare evolution is fairly rapid. Also, the sharpness value in GONG was lower at the time that SOON observed the flare peak (0.0211). This particular case was disqualified for the SOON to GONG comparison in previous sections, due to the difference in peak time, but it is relevant to the event-level comparisons. In the case from 6 September, the flare was occurring near sunset at the SOON, and the elevation angle would have been extremely low. Here it is plausible that GONG would rate the flare as being larger. For the 25 September case, there were two other GONG sites that also observed the flare; one also rated the flare a 3B and the other a 2N. The site that rated the flare a 2N had poorer seeing conditions with a sharpness value of 0.0147. Perhaps the SOON observation also had less than favorable atmospheric seeing conditions, although this is not indicated in the observation of 'fair' quality and no clouds during the flare. There are some instances, however, where the SOON observation quality rating is left unchanged from the default 'fair' yet clouds are noted by the observer in the plain text of the bulletin (see Section 4.2). It is therefore worthwhile to consider not only the SOON quality rating but also the accompanying plain text. For the final flare where there was a difference, on 26 September, there was actually little disparity in brightness between SOON and GONG. Here SOON rated the flare 'brilliant', with an intensity of 3.7 times the background, while GONG rated the flare 'normal', with an intensity of 3.5 times the background.

This is another example of where flare category may differ but actual area or brightness values are similar.

4.4.4 Differences in Peak Flare Times

Once again, a comparison of peak flare times was performed between the two observing networks (Table 17). The average difference in flare peak time was less than

Table 17. SOON to GONG Time Difference Between Sites

Characteristic Between Sites	Number of Occurrences	Average Time Difference (minutes)
Area Categories Match	47	1.5
Area Categories Differ	36	2.2
Brightness Categories Match	49	1.7
Brightness Categories Differ	35	2.1

two minutes, however where there was a difference in area, the average time difference increased to over two minutes. There is some indication of an increased peak time difference being related to a disparity in area or brightness categories, but the difference between peak times of different categories and peak times of the same categories is still rather small. Figures 26 and 27 are similar to Figures 24 and 25 in that they compare SOON and GONG brightness and area measurements, except this time, instead of color coding differing categories, the data points are color coded according to the difference in peak flare time. The red points represent where there difference in flare peak times was greater than or equal to 3 minutes (but less than 10) and the blue points represent where the difference in flare peak times was less than 3 minutes. The plots indicate that while

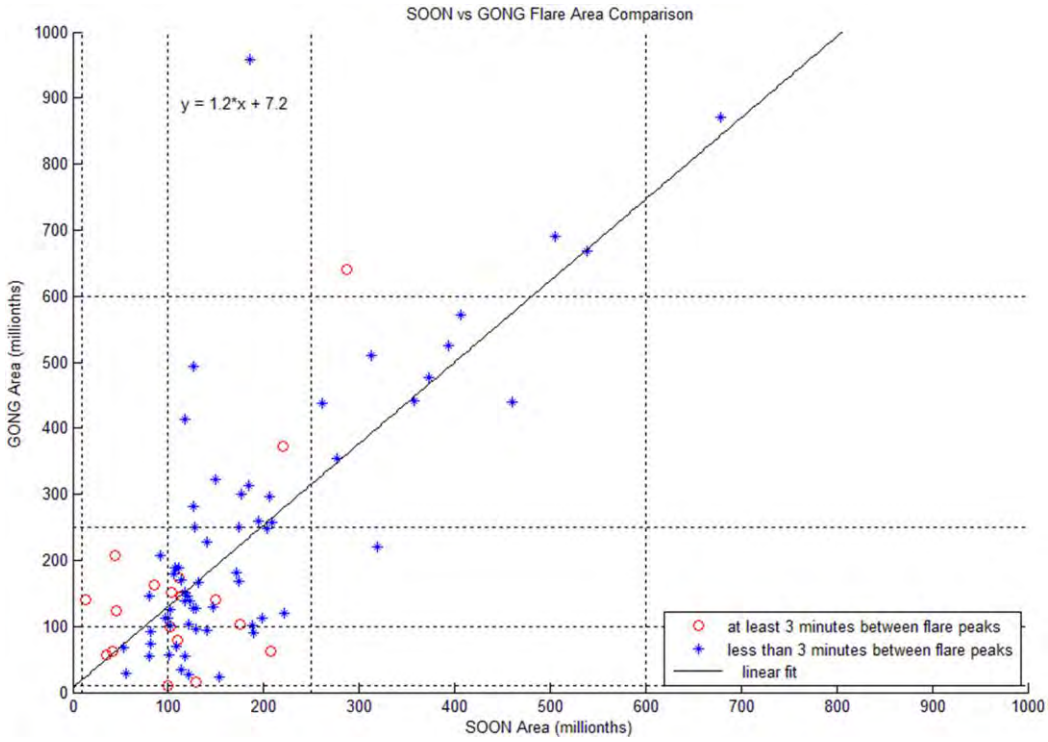

Figure 26. SOON vs GONG Flare Area Comparison – Peak Times Highlighted

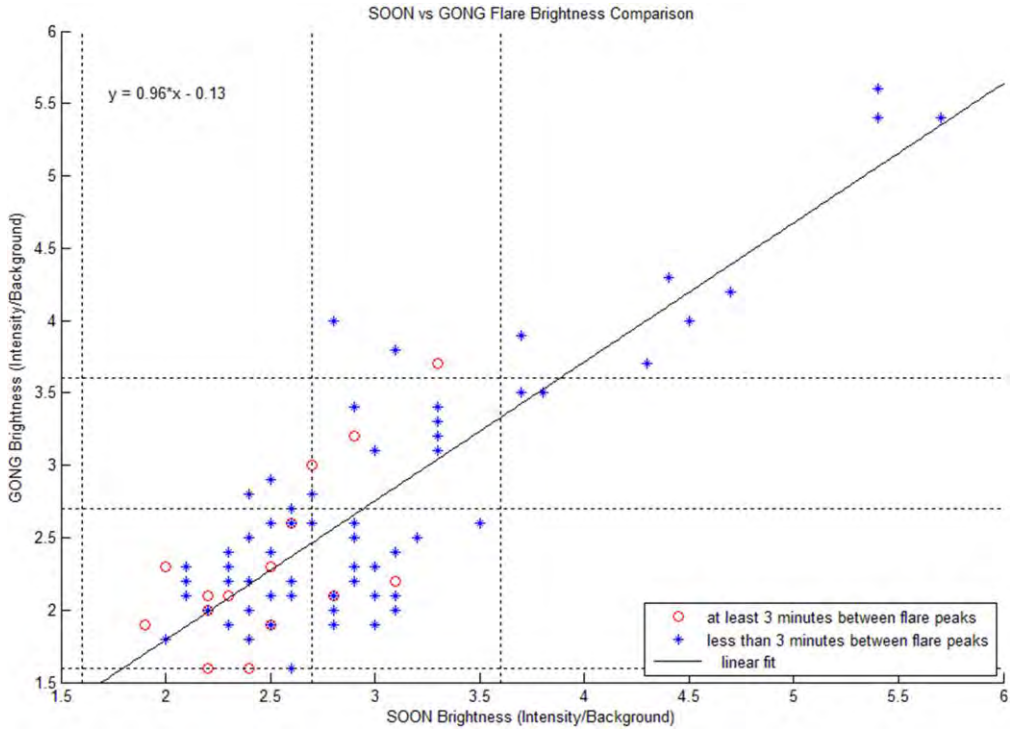

Figure 27. SOON vs GONG Flare Brightness Comparison – Peak Times Highlighted

there are some flares with significantly different area or brightness ratings that also have more than three minutes between peak flare times, there are also many other similar disparate flares that have a smaller difference in peak times between networks.

4.4.5 SOON to GONG Conclusion

The overall variability comparing SOON to GONG flare ratings of flares greater than subflares was 66%, since in 56 of the 85 total flares observed by both networks received different category ratings. Recall that the variability for flares greater than subflares within SOON was 55% and within GONG was 60%. It is not surprising that the SOON to GONG variability not very different. Considering different observing instruments and algorithms were used to calculate flare ratings between the two networks, the 66% variability is acceptable. It does offer justification for higher variability between different networks than within the same network.

For event-level flares the variability was 44%, or 4 of 9 flares, where in five cases there was a match in ratings between networks. In the SOON to SOON comparison there were only three total event-level flares where all three received the same rating, and in the GONG to GONG comparison the variability was 38%, or 3 of 9 flares.

4.5 GONG flares not observed by SOON

Since there are twice as many observatories in the GONG system (six globally) than in the SOON system, there should be a larger total number of flares witnessed by GONG, however this is affected by maintenance down time, seasonal variations in observatory patrol overlap, and local weather conditions. The purpose of this comparison was to see if GONG saw some flares that SOON missed for various reasons. The

thinking was that if there are some significant X-ray flares that were not observed in the SOON networks, it would be worthwhile to analyze the GONG imagery at corresponding times. The most current database for X-ray flares is the GOES-15 X-ray instrument data, archived by the Space Weather Prediction Center (SWPC, 2012). The GOES X-ray instrument continuously monitors the sun for X-ray flares, and a flare rating is assigned according to Table 3 in Chapter 2.

Figures 28 and 29 show how GOES X-ray flux is correlated with SOON flare

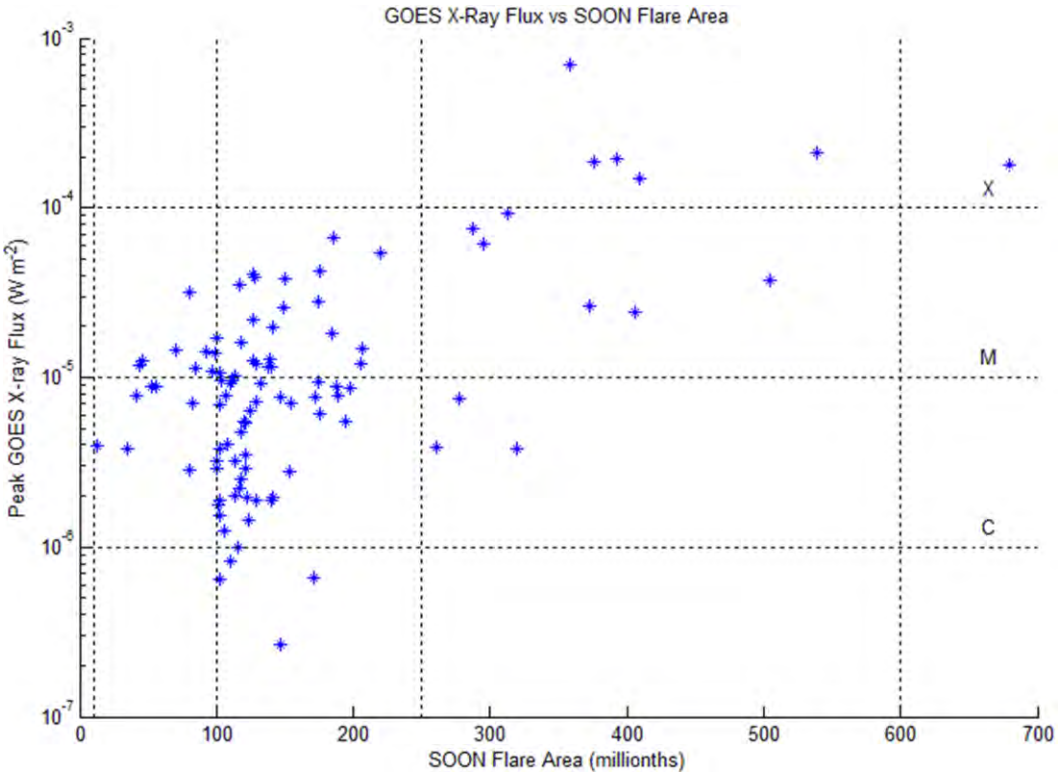

Figure 28. GOES X-ray Flux vs SOON Flare Area

brightness and area for the 100 flares larger than subflares. The plots indicate that there is some relationship between X-ray flux measurements and flare area and brightness,

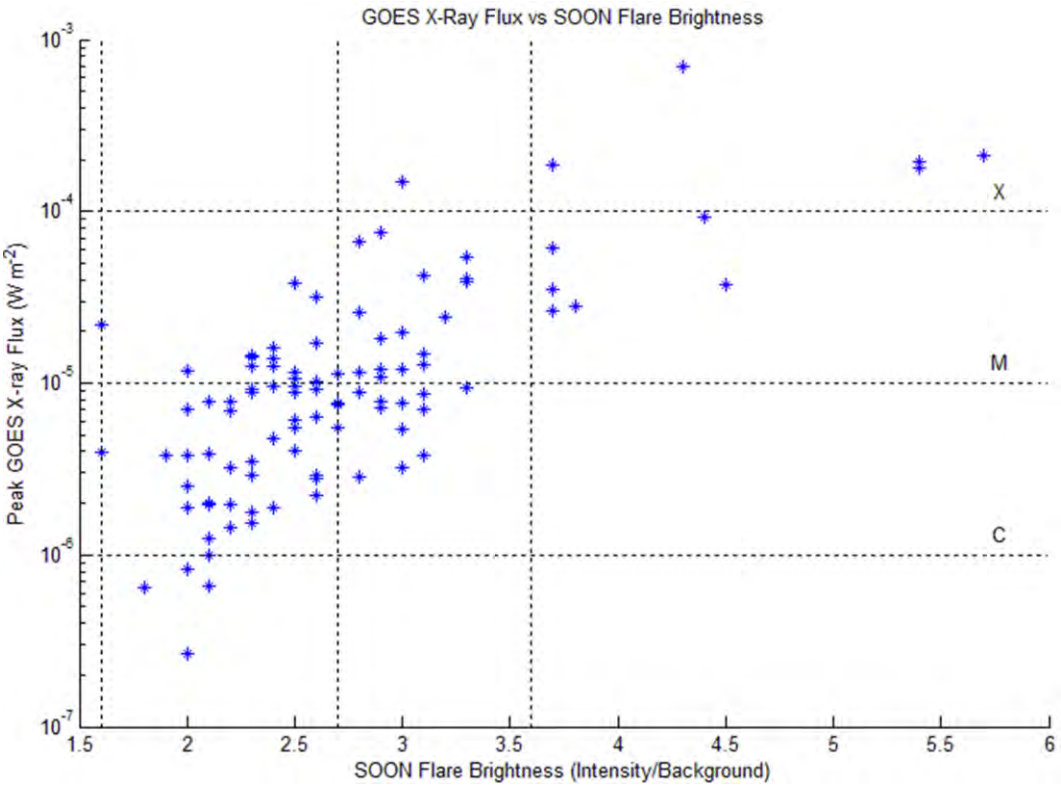

Figure 29. GOES X-ray Flux vs SOON Flare Brightness

however there is still a fair amount of variability. For example, M-class X-ray flares correspond to flare areas ranging from under 50 millionths to over 500 millionths. Likewise, for the same category of X-ray flares, SOON intensity ranges from minimum flare brightness to an intensity of over 4.5 times the background.

The number of X-ray flares as detected by GOES was examined starting during the period of this study, 11 March to 30 November 2011. Of particular interest were the larger M and X-class flares, since these are the most energetic in soft X-rays. Also, the number of these was more manageable compared to the number of C-class flares (over 800). There were however 20 M-class and one X-class flares for which there was no associated SOON optical observation according to the SWPC online archive of flares.

All the GONG imagery for these flares was analyzed to determine if H-alpha flaring could be detected. Of the 21 total, there were 10 optical flares successfully analyzed in the available GONG imagery. Table 18 contains a breakdown of the 21 X-ray flare

Table 18. GONG Flares Not Observed in SOON

Number of Occurrences	Characteristic
9	Limb flare where IDL algorithm could not be run accurately
2	Unavailable or incomplete imagery
10	At least one site observed and flare rating was available

cases, including why in 11 cases a GONG flare rating was not able to be determined.

The area and brightness categories of the 10 flares successfully analyzed are shown in Table 19. If more than one GONG site had imagery available for a particular

Table 19. GONG Flare Ratings Not Observed in SOON

		Brightness				
Importance		**Faint**	**Normal**	**Brilliant**	**Total**	**Percent**
	0	1	0	0	1	10
	1	3	2	0	5	50
	2	1	1	2	4	40
Total		5	3	2		
Percent		50	30	20		

flare, than the site with the largest or brightest flare was used as the rating in the table. The most significant finding of the analysis of the GONG imagery based on the X-ray flare database is that some of the visible flares were found to be of notable size. Of particular interest are the two optical 2B flares that would be considered event-level flares by the Air Force Weather Agency. Table 20 contains some details on these particular flares.

Table 20. GONG Event-level Flares Not Observed in SOON

2011 Date / (hh:mm) UT	GONG Rating	Area (millionths)	Brightness (intensity/ background)	Sharpness
30 Jul / 21:01	2B	263	4.2	0.015
24 Sep / 19:12	2B	326	4.0	0.029

This section demonstrates that there are flares that the GONG network observes that the SOON network does not observe, some of which are significant. Although there were not a large number of flares initially found, future study could incorporate the considerable number of C-class flares as additional candidates. More flares would also likely be detected by using a more robust algorithm that scans the full solar disk for flaring on all archived GONG imagery during the period of this study.

5. Conclusions and Recommendations

The results of the analyses between the SOON and GONG observing systems are discussed in this chapter. Additionally, topics for further research will be presented.

5.1 Summary of Results

The overall conclusion of this research is that GONG is an effective system to detect and categorize solar H-alpha flares with similar capabilities as the SOON system. This conclusion was determined by examining solar flare variability within the SOON system, within the GONG system, and between the two systems.

During this study there were 124 flares of subflare category or greater observed by two SOON sites with an overall variability of 8% due to differences in brightness and/or area category rating. When the flare category was increased to greater than subflares (18 flares), the variability increased to 55%. Finally, for event-level flares (greater than 2B) there was no variability (0%) since in all three flares, both SOON sites rated the flare 2B. In the majority (80%) of the cases when there was a difference between the two sites' observations, the site with the larger solar elevation angle had the larger or brighter flare category rating.

Two or more GONG sites observed 86 flares of subflare category or greater during this time period with an overall variability of 44% due to differences in brightness and/or area category rating. When the flare category was increased to greater than subflares (43 flares), the variability increased to 60%. Finally, for event-level flares, the variability decreased to 38%, or 3 of 8 flares in which there was a difference in brightness or area category. In the majority (95%) of the cases when there was a difference between

the two sites' observations and sharpness was calculated, the site with the higher sharpness had the larger or brighter flare category rating.

There were 85 flares greater than subflares observed by both GONG and SOON with an overall variability of 66% due to differences in brightness and/or area category rating. Of the 36 flares where there was a difference in area category, GONG had the higher area category 53% of the time. Of the 35 flares where there was a difference in brightness category, SOON had the higher brightness category 86% of the time. For event-level flares the variability was 44%, or 4 of 9 flares. GONG observed all SOON event-level flares within one brightness or area category. There were three additional event-level flares detected by GONG that were not observed by SOON networks, and there were no SOON event-level flares that GONG missed. While there are some differences in flare rating between the two networks, most flares rate in the same brightness or area categories and many flares rate the same in both. The variability between flare category rating between SOON and GONG was 66% for flares greater than subflares, which was similar to variability within the GONG network (60%) and within the SOON network (55%). While GONG can provide flare monitoring as effectively as SOON, there are other SOON missions, including sunspot and magnetogram analysis that were not considered in this project.

5.2 Future Research Recommendations

There are three additional research opportunities that are presented that would serve to expand the breadth of this project. For example, this study could be repeated once SOON imagery is calibrated before being archived. Since SOON imagery could not

be used for this study, an actual comparison of SOON images to GONG images may provide more detailed results regarding site conditions and instrumental performance. This study was conducted between 11 March and 30 November 2011. During this time, solar activity was limited, with only nine flares meeting event-level criteria. This study should be repeated to include a greater number of H-alpha flares to confirm these results. Third, the IDL algorithm used to analyze the GONG flares should be improved to analyze flares near the limb.

Bibliography

Air Force Weather Agency (AFWA) (2010). *Space Environmental Observations and Solar Optical Observing Techniques*, AFWAMAN 15-1, AFWA/A3, 12 February 2010.

Air Force Weather Agency (AFWA) (2010). *Space Environmental Observations, Solar Optical and Radio Observing*, AFWAI 15-2, AFWA/A3, 20 April 2010.

ARINC Engineering Services, LLC (ARINC) (2006). *Technical Manual: Solar Observing Optical Network*. TO 31M1-2FMQ7-1. Colorado Springs, 1 January 2006.

Aschwanden, M. J. (2005). *Physics of the Solar Corona: An Introduction with Problems and Solutions*, Springer, Berlin.

Benz, A. O. (2008). Flare Observations, *Living Reviews in Solar Physics*, 5(1).

Carrington, R. C. (1859). Description of a Singular Appearance seen in the Sun on September 1, 1859, *Monthly Notices of the Royal Astronomical Society*, 20, 13-15.

Foukal, P. V. (2004). *Solar Astrophysics*. Wiley-VCH, Weinheim.

Kurokawa, H., et al. (1988). Close relationship between H-alpha and hard X-ray emissions at the impulsive phase of a solar flare, *Astronomical Society of Japan, Publications*, 40(3), 357-367.

Harrison, R. A., et al. (1997). Extreme Ultraviolet Observations of the Solar Corona: First Results from the Coronal Diagnostic Spectrometer on SOHO, *Advances in Space Research*, 20(12), 2239-2248.

Harvey, J. W., et al. (2011). Full-disk Solar H-alpha Images from GONG, *Bulletin of the American Astronomical Society*, 43(5).

Henney, C. J., D. MacKenzie, F. Hill, B. Mills, and J. Pietrzak. (2011). Solar Flare Detection With SWIFT and Real-time GONG H-alpha Images, *Bulletin of the American Astronomical Society*, 43(5).

Hill, F., et al. (1994). The Global Oscillation Network Group Site Survey, *Solar Physics*, 152(2), 351-379.

Kennewell, J. A. (1998). Solar Patrol for The Third Millennium, *Synoptic Solar Physics*, 140, 529-538.

Lang, K. R. (2009). *The Sun from Space*. Springer, Berlin.

Peat, C. (2011). *Heavens-Above GmbH*. Muenchen, Germany. 23 December 2011. http://www.heavens-above.com/

Rosenkrantz, W. A. (2009), *Introduction to Probability and Statistics for Science, Engineering, and Finance*, CRC Press, Boca Raton.

Smith, H., and E. Smith (1963), *Solar Flares*, The Macmillan Company, New York.

Shibata, K. (1998). Reconnection Models of Flares, *Solar Physics with Radio Observations*, *Proceedings of Nobeyama Symposium*, NRO Report 479.

Shibata, K., and T. Magara (2011). Solar Flares: Magnetohydrodynamic Processes, *Living Reviews in Solar Physics*, 8(6).

Space Weather Prediction Center (SWPC) (2012). GOES Satellite Data at the Space Weather Prediction Center. 18 February 2012. http://www.swpc.noaa.gov/Data/goes.html

Tallant, P. E. (1969). A Solar Flare Videometer, *Solar Physics*, 11(2), 263-275.

Tandberg-Hanssen, E., and A. G. Emslie (1988), *The Physics of Solar Flares*, Cambridge University Press, Cambridge.

Temmer, M, et al. (2001). Statistical Analysis of Solar Hα Flares, *Astronomy and Astrophysics*, 375, 1049-1061.

United States Air Force (2009). *Meteorological Codes*, AFMAN 15-124, HQ USAF/A3O-W, 28 October 2009.

Verdoni, A., and C. Denker (2007). The Local Seeing Environment at Big Bear Solar Observatory, *The Publications of the Astronomical Society of the Pacific*, 119(157), 793-804.

Vita

Captain Thomas Wittman graduated from Seton School in Manassas, Virginia in 2001. He entered undergraduate studies at the University of Nebraska-Lincoln (UNL), where, in December 2005, he graduated with a Bachelor of Science Degree in Meteorology. At the time of graduation, he was commissioned a Second Lieutenant through the Air Force Reserve Officer Training Corps Detachment 465 at UNL.

For his first assignment, Captain Wittman was assigned to Barksdale AFB in Shreveport, Louisiana where he served as a lead meteorologist for the 26th Operational Weather Squadron. After two years, he was assigned to the 2d Operations Support Squadron, also Barksdale AFB, where he served first as Wing Weather Officer, then Weather Flight Commander. In May 2010, he entered the Graduate Applied Physics Program, School of Engineering, and Air Force Institute of Technology, to obtain a Master's Degree in physics with a specialization in space weather. Upon graduation, he will be assigned to the Air Force Weather Agency at Offutt AFB, Nebraska.

REPORT DOCUMENTATION PAGE

Form Approved
OMB No. 074-0188

PLEASE DO NOT RETURN YOUR FORM TO THE ABOVE ADDRESS.

1. REPORT DATE *(DD-MM-YYYY)*	2. REPORT TYPE	3. DATES COVERED *(From – To)*
22-03-2012	Master's Thesis	March 2011 – March 2012

TITLE AND SUBTITLE

A Quantitative Analysis of Solar Flare Characteristics as Observed in the Solar Observing Optical Network and the Global Oscillation Network Group

5a. CONTRACT NUMBER

5b. GRANT NUMBER

5c. PROGRAM ELEMENT NUMBER

6. AUTHOR(S)

Wittman, Thomas M., Captain, USAF

5d. PROJECT NUMBER

5e. TASK NUMBER

5f. WORK UNIT NUMBER

7. PERFORMING ORGANIZATION NAMES(S) AND ADDRESS(S)

Air Force Institute of Technology
Graduate School of Engineering and Management (AFIT/EN)
2950 Hobson Way, Building 640
WPAFB OH 45433-7765

8. PERFORMING ORGANIZATION REPORT NUMBER

AFIT/APPLPHY/ENP/12-M11

9. SPONSORING/MONITORING AGENCY NAME(S) AND ADDRESS(ES)

Air Force Research Laboratory- Space Vehicles Directorate
Attn: Dr. Carl Henney
3550 Aberdeen Ave SE Bldg 570 Rm 2222
Kirtland AFB, NM 87117
(505) 853-3057

10. SPONSOR/MONITOR'S ACRONYM(S)
AFRL/RVBXS

11. SPONSOR/MONITOR'S REPORT NUMBER(S)

12. DISTRIBUTION/AVAILABILITY STATEMENT

APPROVED FOR PUBLIC RELEASE; DISTRIBUTION UNLIMITED.

13. SUPPLEMENTARY NOTES

14. ABSTRACT

This study consists of a quantitative comparison of H-alpha solar flare area and brightness as recorded by the Solar Observing Optical Network (SOON) and the Global Oscillation Network Group (GONG) from March 11 through November 30, 2011. The Air Force utilizes the three-site SOON network for H-alpha flare monitoring, while the six-site GONG network, managed by the National Solar Observatory, provides backup H alpha flare monitoring for SOON. A total of 1000 flares were observed and 100 of these were rated larger or brighter than the 0-F category. In the SOON network, 8% of flares observed by two sites had a difference in area or brightness category, or both. In the GONG network, with up to four sites viewing the same flare, 44% of flares observed by multiple sites had at least one site with differences in area, brightness, or both. Of these cases, the GONG site that rated the flare as having the largest or brightest rating also had the highest sharpness 95% of the time. Of the 84 flares larger or brighter than 0 F observed by both networks, area and brightness category ratings were the same 35% of the time. The GONG rating was one category larger or brighter than SOON 26% of the time and the SOON rating was one category larger or brighter than GONG 39% of the time. There was only one case with a two category difference between networks this was attributed to clouds at one site. GONG observed all 9 of SOON's event-level flares while observing three additional that SOON did not observe. Ultimately, GONG observed all SOON flares with the same variability noted when comparing flares observed within the SOON network, and is a reliable source for H-alpha flare observations.

15. SUBJECT TERMS

Solar Flare, SOON, GONG, Space Weather

16. SECURITY CLASSIFICATION OF:			17. LIMITATION OF ABSTRACT	18. NUMBER OF PAGES	19a. NAME OF RESPONSIBLE PERSON
a. REPORT	b. ABSTRACT	c. THIS PAGE			Ariel Acebal, Lt Col, USAF Advisor
U	U	U	UU	91	19b. TELEPHONE NUMBER *(Include area code)* (937) 255-3636, ext 4518 ariel.acebal@afit.edu

Standard Form 298 (Rev. 8-98)
Prescribed by ANSI Std. Z39-18